UCSF
UC San Francisco Electronic Theses and Dissertations

Title
Diversity in the bacterial cytoskeleton: assembly, structure, and cellular mechanisms of AlfA, a plasmid segregating actin from B. subtilis

Permalink
https://escholarship.org/uc/item/6v37w5d5

Author
Polka, Jessica Kathleen

Publication Date
2012

Peer reviewed|Thesis/dissertation

eScholarship.org Powered by the California Digital Library
University of California

Diversity in the bacterial cytoskeleton: assembly, structure, and cellular mechanisms of AlfA, a plasmid segregating actin from B. subtilis

by

Jessica Polka

DISSERTATION

Submitted in partial satisfaction of the requirements for the degree of

DOCTOR OF PHILOSOPHY

in

Biochemistry and Molecular Biology

in the

GRADUATE DIVISION

Dedication

I dedicate this work to my father, who has inspired me with his steadfast approach to engineering, problem solving, and discovery.

Acknowledgements

I would like to thank all members of the Mullins lab, especially Dyche, who has broadened my thinking and shaped my approach to science in many invaluable ways. He has provided both support and the space to explore and develop independence, and I am extremely grateful for this mentorship. Lillian Fritz-Laylin has been inspirational in discussions of both experimental strategies and cognitive approaches to the process of doing science. I am grateful to Natalie Petek and Chris Rivera, excellent colleagues in the bacterial actin side of the lab. My erstwhile rotation advisor, Ethan Garner, has had a tremendously positively influence on this project through thoughtful discussions and helpful advice from a microbiological perspective.

I am grateful to my mentor and collaborator Justin Kollman, who has enriched this project with a structural perspective, and to rest of the the Agard lab. Joe Pogliano and Alan Derman have been extremely generous with their time, reagents, and support. For collaborations relating to this project at the Physiology course at the MBL, I am grateful to Khuloud Jaqaman, Tristan Ursell, Jelmer Lindeboom, Senthil Amurugam, Zita Santos, Abby Vander Heyden, and Dustin Dovala.

I appreciate the support and feedback from my thesis committee: Ron Vale, David Agard, and Orion Weiner. I have also been fortunate for my classmates Colin Dinsmore and Jacob Stewart-Ornstein, who have both provided helpful feedback and a refreshing outside perspective on this work, and for all of my friends and family for their unwavering support.

Contributions

Chapter 2

JOURNAL OF BACTERIOLOGY, Oct. 2009, p. 6219–6230 Vol. 191, No. 20

0021-9193/09/$08.000 doi:10.1128/JB.00676-09

Copyright © 2009, American Society for Microbiology. All Rights Reserved.

The helical reconstruction of the AlfA filament and the determination of helical handedness was performed by Justin Kollman.

Chapter 3

Khuloud Jaqaman and Jelmer Lindeboom performed the first optimization of Gaussian fitting and tracking parameters. Dyche Mullins wrote the instantaneous MSD filter. Justin Kollman produced the homology model.

Chapter 4

Chapter 5

James Kraemer conducted the crystallization screens for Alp7a.

Abstract

Diversity in the bacterial cytoskeleton: assembly, structure, and cellular mechanisms of AlfA, a plasmid segregating actin from *B. subtilis*

Jessica K. Polka

AlfA is a filament-forming actin-like protein in *Bacillus subtilis* that functions to actively partition the large, low copy number plasmid by which it is encoded. Our *in vitro* observations of filament dynamics have revealed a set of kinetic and structural properties (namely constitutive bundling and lack of dynamic instability) that are inconsistent with previously established models for actin-like plasmid segregating proteins such as ParM. To understand the mechanism of AlfA – driven plasmid segregation, we imaged AlfA and its downstream DNA-binding protein, AlfB, interacting with plasmids *in vivo* and *in vitro*. Our live cell microscopy reveals that plasmids can move along existing AlfA structures or track the ends of growing ones, consistent with the idea that the AlfA polymer seen *in vivo* is actually a bundle of multiple filaments. Furthermore, these polymers can form between plasmids to push them apart, prompting us to ask how plasmids alter filament dynamics to generate this specific assembly. To address this question, we purified AlfB and found that it dramatically alters the kinetics and structure of AlfA. AlfB binds to AlfA monomers and polymers, not only increasing the critical concentration of assembly, but also preventing the otherwise very robust bundling of AlfA. The 100bp centromeric DNA region to which AlfB binds, however, rescues bundling and promotes polymerization. These observations lead us to a model of AlfA-driven plasmid segregation wherein bundles of AlfA form specifically

in association with AlfB-DNA complexes. We propose that the intrinsic bundling property of the polymer, normally inhibited by a high concentration of free AlfB in the cytoplasm, functions as a capture mechanism to specifically join DNA-bound filaments to one another. Polymerization in opposite directions, driven by antiparallel bundling, would cause plasmids to be segregated from one another, ensuring their maintenance through cell division.

Table of contents

List of Tables

List of Figures

Chapter 1: Introduction

Living cells need to generate structural and mechanical forces in order to move through their environments, transmit cargo, and maintain their shape. In eukaryotic cells, many of these functions are accomplished through the regulation of the actin cytoskeleton (Pollard 2001). This single polymer is able to participate in processes as varied as phagocytosis, cytokinesis, and cell motility though the spatial and temporal regulation of virtually all aspects of assembly, from nucleotide exchange and nucleation to polymerization, network branching, and severing.

Importantly, the mode of this regulation is shaped by the intrinsic properties of the polymer – for example, because actin nucleates slowly on its own, factors that catalyze nucleation direct assembly of the polymer in the cell. Because individual actin polymers lack rigidity, network branching and crosslinking proteins can tune the rigidity of the network. And furthermore, because of the highly interconnected nature of all these interacting proteins, these factors are highly conserved within commonly studied eukaryotes. As a result of this, most eukaryotic actins are extraordinarily well conserved as well, with 85% sequence identity between yeast and humans, having been entrained through evolutionary history by this conserved network of interactors. Thus, it has low sequence diversity, but many complex regulatory modules that adapt it to a variety of roles in the cell.

Actin was once considered a key delineator between eukaryotes and prokaryotes, but we now know that a huge variety of actin-like proteins exist in bacteria, with each one tuned to a particular function in the cell. For example, MreB is a scaffold for cell wall synthesis

components (Garner 2011), and FtsA localizes to the site of cell division (Fu 2010). ParM is a part of a minimal, mitotic-spindle like apparatus that drives the segregation of large low copy number plasmids, and is our clearest example of a bacterial cytoskeletal filament actually produces forces to move cargos (Campbell 2007). It forms filaments within cells, and these filaments not only push plasmids, but distribute them nonrandomly, so that each daughter cell inherits at least one. This feature relies on the intrinsic dynamic instability of ParM filaments – like eukaryotic tubulin, it undergoes a dramatic conformational switch in response to the transition from ATP to ADP bound states, which causes catastrophic disassembly of the polymer (Garner 2004). Binding to plasmids stabilizes the ends of filaments, and because both ends of the ParM filament need to be stabilized to protect it from catastrophe, only bioriented filaments can elongate all the way across the cell. In this manner, the function of plasmid segregation is enabled by the intrinsic biochemical property of dynamic instability that is encoded within the polymer.

At the time I joined the Mullins lab for my thesis work, AlfA had recently been discovered as the newest class of bacterial actins (Becker 2006). Even though it is as distant in terms of sequence from ParM as either is from eukaryotic actin, it has the same function of segregating large, low copy number plasmids. We wanted to investigate how closely its behavior would mirror that of ParM, despite sequence diversity. Alternately, could the cellular function of DNA segregation be achieved by an entirely different mechanism, which would arise from a set of divergent structural and biochemical properties? In my thesis work, I used the study of this

uncharacterized polymer to understand the breadth of the kinetic, structural, and mechanical repertoire of bacterial actins.

With the goal of understanding the mechanism of plasmid segregation by AlfA, I first expressed and purified AlfA and characterized its assembly properties and structure. This work was published in 2009 and is described in Chapter 2. I found several unique properties of the polymer, namely a natural tendency to bundle and a lack of dynamic instability, and these prompted *in vivo* studies of the interaction between plasmids and filaments, which are described in Chapter 3. Finally, I have returned to *in vitro* biochemistry to dissect the impact of regulatory proteins on AlfA filament kinetics, architecture, and functional segregation. This ongoing work is described in Chapter 4. Finally, in an effort to further flesh out the kinetic, structural, and mechanistic parameter space of bacterial plasmid-segregating actins, I have described a preliminary characterization of a new polymer, Alp7a, in Chapter 5.

References

1. Becker, E. *et al.* DNA segregation by the bacterial actin AlfA during Bacillus subtilis growth and development. *EMBO J* **25**, 5919–31 (2006).

2. Campbell, C. S. & Mullins, R. D. In vivo visualization of type II plasmid segregation: bacterial actin filaments pushing plasmids. *J Cell Biol* **179**, 1059–66 (2007).

3. Fu, G. *et al.* In Vivo Structure of the E. coli FtsZ-ring Revealed by Photoactivated Localization Microscopy (PALM). *PLoS ONE* **5**, e12680 (2010).

4. Garner, E. C. *et al.* Coupled, circumferential motions of the cell wall synthesis machinery and MreB filaments in B. subtilis. *Science* **333**, 222–225 (2011).

5. Garner, E. C., Campbell, C. S. & Mullins, R. D. Dynamic instability in a DNA-segregating prokaryotic actin homolog. *Science* **306**, 1021–5 (2004).

6. Pollard, T. D., Blanchoin, L. & Mullins, R. D. Actin dynamics. *J Cell Sci* **114**, 3 (2001).

Chapter 2: The structure and assembly dynamics of AlfA

Published in

JOURNAL OF BACTERIOLOGY, Oct. 2009, p. 6219–6230 Vol. 191, No. 20

0021-9193/09/$08.000 doi:10.1128/JB.00676-09

Copyright © 2009, American Society for Microbiology. All Rights Reserved.

Jessica K. Polka, Justin M. Kollman, David A. Agard, and R. Dyche Mullins

ABSTRACT

Bacterial cytoskeletal proteins participate in a variety of processes, including cell division and DNA segregation. Polymerization of one plasmid-encoded, actin-like protein (ALP), ParM, segregates DNA by pushing two plasmids in opposite directions and forms the current paradigm for understanding active plasmid segregation. An essential feature of ParM assembly is its dynamically instability, the stochastic switching between growth and disassembly. It is unclear whether dynamic instability is an essential feature of all ALP-based segregation mechanisms or whether bacterial filaments can segregate plasmids by different mechanisms. We expressed and purified AlfA, a plasmid-segregating ALP from Bacillus subtilis, and find that it forms filaments with a unique structure and biochemistry: AlfA nucleates rapidly; polymerizes in ATP or GTP; and forms highly twisted, ribbon-like, helical filaments with a left-handed pitch and protomer nucleotide binding pockets rotated away from the filament axis. Intriguingly, AlfA filaments spontaneously associate into uniform-sized, mixed-polarity bundles. Most surprisingly, our biochemical characterization reveals that AlfA does not display dynamic instability and is relatively stable in diphosphate nucleotides. These results: (i) reveal a remarkable structural diversity among bacterial actin filaments and (ii) indicate that AlfA filaments partition DNA by a novel mechanism.

INTRODUCTION

Bacteria contain multiple filament-forming proteins related to eukaryotic actin (5) These actin-like proteins are adapted to multiple cellular roles, including determination of cell shape (19) arrangement of organelles (21) and segregation of DNA (11) Little is known about the assembly dynamics of most of these proteins or the identities and activities of the factors that regulate them. The widely expressed actin-like protein MreB, for example, has been purified and studied in vitro but its assembly appears to be strongly inhibited by physiological concentrations of monovalent cations, suggesting that its assembly in vivo is facilitated by as yet unknown factors (24) At present, the best-understood actin-like protein is ParM, a plasmid-encoded protein that constructs a bipolar spindle capable of pushing plasmids to opposite poles of rod-shaped cells (26, 4) In contrast to the eukaryotic actin cytoskeleton, whose assembly and architecture are regulated by a variety of accessory factors, ParM dynamics are regulated by a single factor, a complex composed of multiple copies of the repressor protein ParR bound to a DNA locus, *parC (18)* . The ParR/*parC* complex binds the ends of ParM filaments and is pushed through the cytoplasm by filament elongation (26, 4, 15) The ability of ParM to function with such minimal regulation appears to be due to its unique assembly dynamics, which are dramatically different from those of eukaryotic actins. One of the most important differences is that ParM filaments are dynamically unstable (14) That is, similar to eukaryotic microtubules, they can exist in one of two states: stably growing or rapidly (catastrophically) shrinking. This property is required for the ability of ParM to segregate DNA in vivo and appears to solve several fundamental problems associated with DNA segregation. First, spontaneous disassembly of the polymer overcomes the

need for an accessory factor to take filaments apart. Second, because filaments bound to ParR/*parC* complexes are selectively stabilized, the catastrophic disassembly of unattached filaments provides excess monomers that can preferentially elongate them. This is significant because, if the stability of attached and unattached filaments were similar, the concentration of free ParM monomers would equilibrate at a level incapable of promoting DNA segregation. And finally, pairs of plasmids appear to find each other via a search-and-capture mechanism (4, 15) that is dramatically enhanced by the continual growing and shortening of filaments attached to single plasmids (17)

Because we have little information on the dynamics of other actin-like proteins, it is unclear to what extent ParM's behavior reflects general properties of bacterial actins versus specific adaptations to its role in DNA segregation. Furthermore, it is unclear whether all plasmid-segregating actins employ the same dynamic instability-based strategy to find and transport DNA molecules. To better understand the structural and functional diversity of bacterial actins, we studied a second, recently discovered plasmid-segregating actin-like protein, AlfA (1) AlfA is part of an operon (*alf*), located close to the origin of replication of a ~70kb, low-copy plasmid, pLS32. This plasmid was initially isolated from a subspecies of *Bacillus subtilis*, *Bacillus natto*, used in soybean fermentation (34) but a similar plasmid with an identical *alf* operon is also found in a colony-forming laboratory strain of *B. subtilis*, NCIB 3610 (33, 7) The function of these plasmids is cryptic. They are present at only 2 to 3 copies per chromosome equivalent (34) and the maintenance of their derivatives requires both AlfA and a downstream gene, *alfB (1)*

Pogliano and co-workers (2006) identified AlfA as a member of the actin superfamily based on the presence of a conserved nucleotide binding fold,[15] although the sequence of AlfA is as different from that of ParM and MreB as all three are from conventional eukaryotic actin (~20% identity). These authors also showed that fluorescent derivatives of AlfA form a single filamentous structure running along the long axis of the cell. Photobleached filaments recover from both ends in approximately one minute, indicating that the structures are composed of multiple, dynamic filaments (1) By analogy with the ParR/*parC* complex, AlfB might be a DNA binding protein that couples AlfA assembly to plasmid movement. To date no centromeric sequences involved in segregation have been identified in this plasmid.

We expressed and purified AlfA and characterized its assembly dynamics by light scattering, high-speed pelleting, and fluorescence microscopy, and we determined the structure of AlfA polymers by high resolution electron microscopy. We found that, in the presence of ATP and GTP, AlfA forms two-stranded helical filaments and filament bundles. Like ParM, AlfA filaments are left-handed two-start helices but, otherwise, their filament architecture is quite different. AlfA filaments appear more tightly twisted and ribbon-like, and AlfA subunits have a significantly different orientation with respect to the filament axis. Unlike other actin-like proteins described thus far, AlfA spontaneously forms regularly sized, mixed-polarity filament bundles, driven by electrostatic interactions between filaments, even in the absence of molecular crowding. Finally, AlfA shows no evidence of the dynamic instability crucial to the function of ParM. Thus, AlfA

assembles into a unique structure with a unique set of biochemical and structural properties, suggesting a novel mechanism for DNA segregation.

MATERIALS AND METHODS

Expression and purification of AlfA

We designed a codon-optimized gene encoding the amino acid sequence for AlfA (DNA 2.0, Gene Designer). This gene was synthesized (Bio Basic) and cloned into pET20b with and without the addition of a 3 amino acid (KCK) tag to the C-terminus for use in maleimide labeling reactions. Our cloning strategy also introduced an additional M at the N-terminus of both constructs used in this study. However, we believe this to be irrelevant because AlfA expressed with a single M performed identically in a low-ATP light scattering assay (data not shown). Restriction sites were chosen to exclude pelB leader peptide and His tags from the expressed ORF, which was confirmed by sequencing. C43 cells were transformed, grown at 37º C to an OD600 of 0.8, and induced with 0.5mM IPTG for 14 hours at 20º C. Cell pellets were frozen at -80º C, thawed, and resuspended in depolymerization buffer (100mM KCl, 25mM Tris HCl pH 7.5, 1mM DTT, 1mM EDTA) before lysis with a microfluidizer and clarification by high-speed centrifugation. Ammonium sulfate cuts were taken from the high-speed supernatant, with the 30-50% pellet being resuspended in polymerization buffer (100mM KCl, 25mM Tris HCl pH 7.5, 1mM DTT, 1mM $MgCl_2$). After preclearing the resuspended ammonium sulfate pellet, ATP was added to a final concentration of 5mM and polymer was pelleted by centrifugation at 80,000 rpm for 15 minutes. This polymerized pellet was then resuspended and allowed to dialyze for 8 hours in depolymerization buffer with the addition of 5mM EDTA, after which time it was gel filtered over a Superdex 75 column equilibrated in depolymerization buffer. Peak fractions were dialyzed into polymerization buffer containing 20-50% glycerol and frozen.

Electron microscopy

We polymerized wild type AlfA by addition of 5mM ATP in polymerization buffer, and applied 4 µl of the reaction to glow-discharged 200 mesh carbon formvar coated copper grids at 25º C. After washing with three drops of polymerization buffer, grids were negatively stained with three drops of 0.75% uranyl formate. Samples were imaged at 25º C with a Tecnai T12 microscope at an acceleration voltage of 120kV at 52,000X. Images were recorded on a Gatan 4k x 4k CCD camera.

Image processing

Non-overlapping segments of two-filament bundles were boxed out in 396 Å boxes using the program Boxer, part of the EMAN software suite (23) Reference-free class averages were calculated with the startnrclasses program from EMAN.

For the single filament reconstruction, the defocus of each micrograph was determined using CTFFIND (25) and the entire micrograph was corrected by phase-flipping. Straight sections of single AlfA filaments were identified using Boxer; subsequent image processing was performed in SPIDER (13) Segments were boxed out along the filament in 265 Å boxes that overlapped by 90% along the helical axis. Each particle was binned two-fold to a final pixel size of 4.4 Å. Iterative helical real space reconstruction was used to refine the helical structure and

symmetry parameters using a featureless cylinder as an initial model (8) Forty rounds of reconstruction at a final angular increment of 3° were carried out for each reconstruction.

Reconstructed volumes were viewed, and manual placement of crystal structures was performed, with Chimera (30)

Labeling of AlfA with fluorescent dyes and biotin

Glycerol and DTT were removed by PD10 or Nap5 salt exclusion columns equilibrated in polymerization buffer without DTT. We incubated AlfA-KCK in a 1:1-1:2 molar ratio with a maleimide label for 15 minutes at 25º C. The reaction was quenched with 10mM DTT, and free label was removed by gel filtration over G25 resin in the case of Cy3 and Alexa 488 labels. Protein was frozen in 0.2M sucrose. The labeling efficiency was 60-100%.

High-speed pelleting assays

We made serial dilutions of wild type AlfA in polymerization buffer and determined their concentration using absorbance at 280nm. Immediately after addition of 5mM ATP, samples were spun at 80,000 rpm in a TLA 100.4 rotor at 25º C for 15 minutes. Supernatants were recovered and separated by gel electrophoresis on 4-12% polyacrylamide gradient gels. Gels were stained with SYPRO red and scanned with a Typhoon variable mode imager before

quantitation with ImageQuant TL. The critical concentration was taken as the x-intercept of the plot of material missing from the supernatant.

Light scattering assays

Right angle light scattering was conducted by mixing wild type AlfA with ATP or GTP in polymerization buffer (at either 100mM or 1.8M KCl) in a SFA-20 rapid mixer (Hi-Tech) in a digital K2 Fluorimeter (ISS, Champagne IL) at an excitation wavelength of 320nm. To calculate the critical concentrations, maximum intensity values were collected from 5-second moving averages of background-subtracted 300-second traces. The maximum intensity was plotted against concentration as measured by absorbance at 280nm, corrected for dilution. The critical concentration was taken as the x-intercept of this plot.

Phosphate release assays

Assays were performed using the EnzChek phosphate assay kit (Invitrogen) in an Ultrospec 2100 Pro spectrophotometer controlled with SWIFT II software (GE Healthcare Life Sciences). A360 values were converted to Pi by use of a phosophate standard.

Total internal reflection fluorescence (TIRF) microscopy

We used a Nikon Eclipse TE2000-E inverted microscope equipped with an Andor iXon+ EM digital camera and a CrystaLaser 100mW 542 nm solid state laser. Microscopy chambers were constructed from glass which was base-washed in 0.5M KOH and treated with 1% APTES. After assembly, chambers were treated with 9 mg/mL PEG-NHS and 1 mg/mL biotin-PEG-NHS. Before use, chambers were treated with 2µM streptavidin.

RESULTS

AlfA filaments spontaneously assemble in ATP and GTP and self-associate to form mixed polarity bundles.

We initially attempted to express AlfA in *Escherichia coli* using an *E. coli* expression vector containing the native *alfA* gene. Despite systematic variation of expression conditions (temperature and time of induction, cell density, E. coli strain, concentration of IPTG, etc.) we never observed significant expression of AlfA in *E. coli*. More careful analysis of the *alfA* sequence revealed a significant number of codons rarely found in *E. coli* genes. We therefore redesigned the gene (Gene Designer, DNA 2.0; and BioBasic) optimizing codon usage for *E. coli* and observed high levels of AlfA expression. To purify AlfA we used a scheme similar to one we used for ParM that relies on ATP-dependent pelleting of the protein in the ultracentrifuge (14)

The success of our purification scheme suggested strongly that AlfA polymerizes upon addition of ATP. To see what sort of polymers AlfA forms, we mixed 5μM AlfA with 5mM ATP, negatively stained samples with uranyl formate, and imaged them by electron microscopy. We observed filamentous bundles with an approximate width of 20nm and an internal structural repeat every 100nm (Figure 1A, arrowheads). Many bundles have blunt ends, while others appear splayed, demonstrating that the bundles are composed of individual filaments. These single filaments are approximately 7nm in diameter and appear to be double-stranded, similar to actin, ParM, and MreB. Similar to the previously characterized plasmid actin, ParM, AlfA filaments and bundles can be assembled by addition of either ATP or GTP, with no appreciable differences in morphology. Unlike the dynamically unstable ParM, however, AlfA filaments can

also assemble in the presence of ADP and GDP (figure S1). The small bundle in Figure 1B is composed of four filaments, suggesting that the larger bundles seen in Figure 1A contain at least twice this number.

To better understand the relative orientations of filaments in the bundles, we generated reference-free averages of two-filament bundles; in one of these averages the filaments appear to run antiparallel to one another (figure 1C). The antiparallel orientation of the filaments was confirmed by reference-based matching to projections of the single filament reconstruction (see below). This configuration suggests that the larger bundles contain filaments with a mixture of polarities.

AlfA bundles form spontaneously due to electrostatic interactions between filaments. Bundling was not due to molecular crowding or depletion interactions since we collected EM images in the absence of crowding agents such as methylcellulose. Unlike actin paracrystals(20), AlfA bundles appear even at low concentrations of $MgCl_2$ (down to 100μM, data not shown). High concentrations of KCl, however, support polymerization but efficiently suppress formation of AlfA filament bundles. At 0.1M KCl virtually all AlfA is present in bundles. At 1.0M KCl, about half of the structures seen are single filaments, with bundles appearing smaller, and at 2.0M KCl, almost all AlfA bundles are disassociated into single filaments. Even in 2.0M KCl, however, a few small bundles can be observed (figure 1D). Concentrations of KCl above 0.1M are required for efficient polymerization. Below 0.1M KCl, fewer bundles are observed on the grid, and at 0.01M KCl, only monomer is seen (figure 1D).

We next observed the assembly of AlfA bundles by total internal reflection fluorescence (TIRF) microscopy. For these experiments we tethered AlfA filaments to biotin-PEG-streptavidin coated coverslips by including 10% biotin-labeled AlfA in the reaction. We visualized the filaments by including 20% Cy3-labled AlfA. All experiments were performed in the absence of crowding agents. At steady state, five minutes after addition of ATP under the same conditions where few single filaments are observed by EM (0.1M KCl), AlfA forms filamentous structures of varying size and intensity (figure 2A). The variation in fluorescence intensity of filamentous structures in the same field suggests that they are composed of varying numbers of filaments. Although the bundles seen by EM appear fairly uniform in size, they often appear grouped laterally alongside other bundles (figure 1A and S2), and the structures seen by TIRF may represent such groups of many bundles running parallel to one another.

Consistent with the ability to polymerize in ADP or GDP, time lapse imaging of AlfA at steady state reveals that bundles do not undergo cycles of growth and shrinkage, characteristic of dynamic instability. Instead, they persist for many minutes without changing in length, although they do undergo stepwise changes in intensity that may be due to bundles recruiting filaments from solution, disassociating from the coverslip, or photobleaching.

To understand how AlfA bundles grow to reach their steady state size, we observed the onset of filament assembly by flowing AlfA into microscopy cells immediately after addition of ATP. Bundles can be observed to grow over a period of several minutes by apparent bidirectional elongation (figure 2B). However, bundles are also frequently seen to anneal to one another (figure 2C) and most growing structures increase in size predominantly by annealing to

filaments from solution. In kymographs, these events appear as stepwise increases in bundle length and intensity (arrows in figure 3D). The majority of the filaments we observed grow by lateral annealing, and the adhesion of filaments from solution to existing seeds occurs much more frequently than we would expect for random landing on the coverslip based on the rate of filament adhesion to unoccupied places on the coverslip. Given that annealing events are responsible for the majority of the growth under our assay conditions, it is difficult to determine elongation rates for single AlfA filaments.

Spontaneous AlfA assembly is rapid under bundling and non-bundling conditions, and shows no evidence of dynamic instability.

We next examined the kinetics of AlfA polymerization by light scattering. Spontaneous assembly of AlfA is much more rapid than that of conventional eukaryotic actin, and more similar to that of plasmid-encoded ParM. In saturating (5mM) ATP, AlfA at concentrations above 3μM assembles rapidly, reaching equilibrium approximately in one minute after addition of nucleotide (Figure 3A). A lag in polymerization kinetics at early time points suggests that, like actin and ParM, AlfA assembles via nucleation-condensation. Data collapse of these curves after normalization of intensity (100%) and time ($t_{½}$) indicates that assembly occurs via a single mechanism at all concentrations (figure 4D).(12) The signal generated by 4 μM AlfA in low concentrations of ATP (figure 3C) does not show a rapid decrease in intensity after an initial burst of polymerization, as is seen for ParM.(14) Rather, the signal decreases slowly, and only in extremely low concentrations of ATP (12.5μM, approximately a 3:1 molar excess over AlfA in

this experiment) do we observe complete depolymerization within a five minute time course. At half this concentration of ATP (6.25μM, approximately 1.5:1 molar excess), we observe no polymerization.

AlfA assembles with similar kinetics in saturating GTP (figure 3B), but appears to be less stable in low concentrations of GTP than ATP. We say this because intensity decreases more rapidly in low concentrations of GTP, and because the GTP concentration threshold for observing AlfA polymerization is higher. No AlfA, for example, polymerizes in 25μM GTP (figure 3D), while we observe a significant signal from the same concentration of AlfA in 25μM ATP (figure 3C).

We used light scattering (supplemental figure 2B) and high speed pelleting (table 1) to estimate critical concentrations of AlfA assembly in ATP, ADP, AMP-PNP, GTP, and GDP. Both methods indicate that AlfA has similar critical concentrations in ATP and GTP. Furthermore, high speed pelleting demonstrates that critical concentrations in ADP and GDP are within an order of magnitude of those in ATP and GTP. The ratios of the critical concentrations in di- and tri-phosphate nucleotides are comparable to the ratio of ADP and ATP critical concentrations of conventional actin but strikingly different from the very high ratio of ParM filaments (14) The relative stability in diphosphate nucleotides is consistent with the lack of dynamic instability observed by TIRF microscopy.

To remove potential effects of bundling on filament dynamics, we compared the behavior of AlfA in low salt buffers that permit bundling to its behavior in high salt buffers that favor single filaments (figure 4). In buffers containing 1.8M KCl, AlfA pellets in ATP, ADP, GTP,

and GDP, with critical concentrations 2- to 4-fold higher than in low salt (table 1), suggesting that AlfA does not exhibit dynamic instability under conditions that dissociate bundles. The intensity of light scattering is much lower in high salt (1.8M KCl), likely because the bundles scatter light more effectively than single filaments, making direct comparison between the two conditions difficult. We compared the polymerization of 3.8μM AlfA at 0.1M KCl to 7.4μM AlfA in 1.8M KCl (figure 4A). Given the critical concentrations measured by light scattering (table 1), both reactions produce equivalent (~1μM) quantities of polymer at steady state. However, it is apparent that the low salt reactions produce a far stronger signal.

We next compared the rates of polymerization in high and low salt. Based on the different critical concentrations, we chose starting concentrations of AlfA that would produce similar concentrations of polymer at steady state under the two conditions (3.1μM in 0.1M KCl and 7.4μM in 1.8M KCl). We collected complete light scattering curves at instrument settings appropriate for each condition, and normalized the resultant traces to their maximal intensity. This comparison demonstrates that AlfA polymerization is slightly slower in 1.8M KCl than in 0.1M KCl (figure 4B).

We used kinetics to investigate the mechanism of AlfA filament assembly. We first estimated the size of the AlfA nucleus, defined as the smallest oligomer to which monomers add with approximately the same affinity as stable filaments, under bundling and non-bundling conditions. We did this several ways, first by plotting the concentration dependence of the maximal velocity of spontaneous polymerization as described by Nishida and Sakai (27). The maximal velocity of each light scattering curve was normalized by its maximal intensity. We

plotted the log of this value against the log of the AlfA concentration (figure 4C) and fit it to a straight line. In the Nishida and Sakai formalism, the slope of this line is equal to the nucleus size divided by two (see Supplementary Material for derivation). Regardless of whether the analysis was performed with low salt (0.1M KCl) or high salt (1.8M KCl) data, the slope of the line generated is approximately 2, suggesting that AlfA polymerizes from tetrameric nuclei in both cases. Thus, AlfA assembles by the same mechanism in both buffer conditions, although nucleation appears somewhat slower in high salt.

We also estimated the nucleus size from the kinetics of assembly at early time points. Using a method described by Flyvberg and Leibler (12) we normalized light scattering data by their maximum intensity and half-times, and observed a collapse of all the data onto a single curve, regardless of the concentration of AlfA (figure 4D). This type of "phenomenological scaling" indicates that the same mechanism governs polymer assembly at different protein concentrations. On a log/log scale the slope of the early time plots of the normalized data is related to the number of steps in the nucleation mechanism. In this case, we estimate a slope of two, consistent with a trimeric nucleus. The slight nonlinearity of the light scattering signal at the earliest time points when the average polymer length is small means that the Nishida and Sakai formalism may provide the more accurate estimate. Nevertheless, the two independent methods argue that the size of the AlfA filament nucleus is between 3 and 4 subunits.

Finally, we numerically simulated AlfA assembly using the Berkeley Madonna software package. For the simulation, we assumed a nucleus size of four, a filament elongation rate similar to those of actin and ParM, and a disassembly rate consistent with measured critical

concentrations. We varied the rate constants for formation of AlfA dimers, trimers, and tetramers to obtain a best fit to light scattering data sets collected at four different AlfA concentrations (from 7.9 to 14.1 μM). All data used for fitting were collected in high salt (1.25 M KCl) to minimize nonlinearities associated with strong light scattering from bundles. Global, nonlinear, least-squares fitting yielded a single set of rate constants that fit the data at all concentrations (supplemental figure 3). From this analysis we estimate an affinity for AlfA dimerization of ~10 mM. This is approximately 500-fold higher than the estimated affinity of a conventional actin dimer (32).

We used a coupled enzyme assay to monitor ATP hydrolysis and phosphate release from 5μM AlfA in both limiting (50μM) and saturating (5mM) ATP (figure 5). At early time points both ATP concentrations produce similar curves while, at steady state, when the light scattering signal is unchanging, phosphate release is faster in saturating ATP (figure 5A vs. C). At early time points, in both low and high concentrations of ATP, phosphate release keeps pace with polymerization and we observe almost no lag between the two curves. It is not possible from these data to obtain an accurate value for ATP hydrolysis and phosphate release but we can place lower bounds on both processes of around 0.4 sec^{-1}. This is significantly faster than the rate of phosphate dissociation from conventional actin or previously characterized actin related proteins (3, 6, 22)

We compared ATP hydrolysis and phosphate release of AlfA with that of 5μM ParM at the same ATP concentrations. In both concentrations of ATP, the initial burst of phosphate release by ParM lags significantly behind polymerization (figure 5A and 5D). In saturating ATP,

the steady state rate of phosphate release by ParM is faster than that of AlfA (figure 5A, B), indicating that, in the steady state plateau phase, when total polymer levels are constant, the flux of ParM subunits through filaments is faster AlfA.

Reconstruction of the AlfA filament structure: AlfA forms left-handed filaments with an architecture distinct from that of ParM.

We polymerized AlfA in the presence of 1.25M KCl to produce EM grids rich in single filaments. We first collected electron micrographs at multiple tilt angles and generated three-dimensional tomograms of individual AlfA filaments to establish the handedness of the long-pitch helix (figure 6H). These tomograms revealed that, like ParM, AlfA filaments are two stranded helical polymers with a left-handed pitch. As a control, the right-handedness of the actin helix was confirmed in parallel experiments (figure 6I) (16)

We determined the structure of single, unbundled AlfA filaments by iterative helical real space reconstruction (IHRSR), a single-particle reconstruction approach to helical structure determination (9, 8) We first collected a set of fifty micrographs of negatively stained AlfA filaments at defocus values from 0.8 to 1.6 µm (1.1 µm average), as determined with CTFfind, and corrected for the CTF by flipping the phases of the whole micrographs. Filaments were extracted from corrected micrographs in 265 Å segments (figure 6A), with 90% overlap of boxes along the filament length. The high degree of overlap enables us to make full use of the helical symmetry during refinement of the structure. The approximate orientation of each filament was

recorded to use as a constraint on the segment rotation during the alignment procedure. In total, we extracted and used 42,547 segments for the reconstruction.

As an initial model for projection matching, we used a featureless cylinder. Reference projections were generated at 3º intervals perpendicular to the cylinder axis. We carried out forty rounds of iterative projection matching alignment and reconstruction, and in each round a search was performed for the optimal helical symmetry, defined as the rotation around and translation parallel to the helical axis between adjacent subunits, as described by Egelman (8) This approach requires an initial estimate of the helical symmetry parameters, and it is an indication of the robustness of the reconstruction that the refinement of the symmetry parameters converges when different initial estimates are used (supplemental figure 4). After rejection of segments with excessive shifts parallel to the helix axis or with rotations deviating from the initial estimates of the helical axis orientation, 36,158 segments were included in the final reconstruction.

In addition to the convergence of symmetry parameters from different starting values, there are several other indicators of the reliability of the reconstruction. Average images of particles with the same refined orientations are nearly identical to reprojections of the final model in the same orientation (figure 6 B,C), showing that our model is self-consistent. More convincingly, an average power spectrum of 2000 non-overlapping segments has the same features as the power spectrum of the reconstruction (figure 6 D,E). While the resolution indicated by the FSC 0.5 criterion is 15 Å (supplemental figure 5), the lack of surface detail suggests that the effective resolution may be somewhat lower; this is likely due to the use of

negative stain as a contrast agent. Finally, a parallel reconstruction of an *Acanthamoeba* actin filament using the same sample preparation and reconstruction techniques yielded a structure with clearly identifiable features of conventional eukaryotic actin.

The architecture of the AlfA filament is significantly different from that of previously described actins. The subunits in the AlfA filament are related by a rotation of 157º and a translation of 25 Å along the helical axis. The filament is two stranded, with a rotation of 46º and a translation of 50 Å between subunits in each strand (figure 6F). While the translation between subunits is similar to that of ParM, the rotation is 18º greater in AlfA than in ParM (28) At higher contour levels, the map clearly shows the separation between strands and suggests boundaries between AlfA subunits (figure 6G). The helix is relatively open, with minimal buried surface between the two strands. The overall shape of the helix is more ribbon-like than either conventional actin or ParM, with a maximum width of ~100 Å and minimum width of ~45 Å.

We made several attempts to fit the crystal structures of AlfA homologs into the EM reconstruction. The crystal structures of actin (PDB 2BTF)(31) and nucleotide-bound ParM (PDB 1MWM)(11) did not fit well into our AlfA filament structure. However, a reasonable fit was obtained with the apo conformation of ParM, in which the ATP binding cleft is opened by about 25º relative to the apo state (PDB 1MWM)(11). In the best fit, the ATP binding cleft of the crystal structure is tilted roughly 45º relative to the direction of the helix axis (figure 7A). Of course, the reliability of this fitting is limited by both the distant relationship between ParM and AlfA and by the resolution limitations inherent in negative stain reconstructions, and the assignment of the AlfA orientation within the filament should be considered preliminary. A

more detailed understanding of the orientation of the individual AlfA subunits will require a higher resolution cryo-EM reconstruction of the filament.

The overall symmetry of the AlfA filament is distinct from both ParM and actin filaments. Recent reconstructions of ParM filaments in both the apo and ADP conformations have a rotation of 30º between subunits along each strand (figure 7B,C; E. H.Egelman, personal communication). The actin filament has a rotation of 27º between subunits, but in the opposite direction, producing a right-handed helix (figure 7D)(29). By contrast, AlfA has a twist of 46º between subunits, producing a more twisted helix (figure 7A). Furthermore, the AlfA filament appears to make fewer contacts between the two strands, producing a filament with a more open architecture than ParM or actin. These differences in the overall architecture may be explained in part by the apparently unique orientation of the AlfA protomer within the filament: in the AlfA filament the ATP-binding cleft seems to be tilted by about 45º relative to the helical axis, whereas in both ParM and actin the ATP binding cleft is nearly parallel to the helical axis.

DISCUSSION

Two major results of our study – 1) that AlfA filaments are not dynamically unstable, and 2) that they spontaneously form mixed-polarity bundles – provide a molecular basis for previous observations made by Pogliano and co-workers *in vivo (1)* These authors found that, unlike ParM, which forms short-lived filaments in *E. coli (4)* AlfA forms stable structures that run from pole-to-pole in *B. subtilis* and display no evidence of catastrophic disassembly. These data are consistent with our discovery that, like eukaryotic actin, AlfA can polymerize in the presence of ADP with a critical concentration only fourfold higher than in ATP. Furthermore, by TIRF microscopy, fluorescent AlfA filaments are stable and do not undergo obvious phases of growth and shortening. Together, these data argue strongly that, unlike ParM, AlfA filaments are not dynamically unstable. When Pogliano and co-workers photobleached fluorescent AlfA structures *in vivo,* they found that the bleached region recovered symmetrically from both sides, suggesting that, *in vivo,* AlfA forms bundles of multiple (possibly treadmilling) filaments. The fact that the new filaments follow exactly the track of the original bleached structure suggests close lateral association between the filaments. This fits with our electron microscopy of purified AlfA, which reveals that, in the presence of ATP or GTP, the protein has a strong tendency to form tight, mixed-polarity filament bundles. Furthermore, using TIRF microscopy, we directly observed labeled AlfA structures zippering together into larger bundles. Together, our results and those of the Pogliano group demonstrate that the i*n vivo* and *in vitro* assembly dynamics of AlfA are unique, and they strongly suggest that the mechanism of AlfA-dependent DNA segregation is significantly different from the previously characterized ParM-dependent process.

Dynamic instability of ParM filaments provides a mechanism for balanced plasmid movement. Because the filament is unstable at both ends, only bivalently attached filaments are competent to elongate, and the movement of one plasmid to a pole is always coupled to the movement of a second plasmid to the opposite pole. Our finding that AlfA is not dynamically unstable raises important questions about AlfA-dependent DNA segregation. It is easy to imagine elongating AlfA filaments aligning with the long axis of a cell and forming a track running from pole to pole. Here is the mystery: if plasmids are not required for filament assembly or stability, how does such a track segregate plasmids? First, plasmids must somehow interact with AlfA filaments. This interaction might be mediated by accessory factors, possibly located in nearby open reading frames in the pLS32 plasmid. One potential regulator, *alfB*, is a gene directly downstream of *alfA* that is also required for plasmid maintenance (1) Based on homology to transcription factors, *alfB* is predicted to encode a DNA binding protein. The role of AlfB in DNA segregation may be similar to that of the Type II segregation factor ParR, which attaches plasmid DNA to the growing ends of ParM filaments (4, 26) Another potential regulator might be encoded by a previously undescribed open reading frame downstream of AlfB that we call "*alfC*." This ORF is very short and has no obvious homology to known proteins. It is unknown whether AlfC interacts with AlfA, and further studies will be required to determine whether it plays a role in plasmid segregation.

The two most general modes by which a plasmid could interact with an AlfA filament are: 1) end binding and 2) side binding. If plasmids (perhaps via AlfB) bind to the end of AlfA filaments, they may be pushed poleward by assembly of filaments growing along the existing

bundle (figure 8B). Alternately, plasmids may bind to the side of the filaments and be carried in one direction or the other by filament treadmilling. Both models explain how one plasmid might find a pole, but neither explains how two plasmids could be partitioned to opposite poles. We know from in vivo experiments that AlfA does, in fact, partition plasmids rather than simply place them at the poles (1) One potential solution to this problem would be a mechanism for ejecting supernumerary plasmids from an occupied pole and encouraging them to travel to the other pole. Such a mechanism could be produced by strictly limiting the number of polar plasmid binding sites. These sites could either be on the ends of AlfA filaments or provided by host cell factors. The existence of host cell anchors is plausible since pLS32 is found only in Bacillus species and one Bacillus gene, *racA*, is already known to help maintain pLS32 during sporulation. Normally, RacA helps anchor the bacterial chromosome in the forespore (2, 36) but deletion of the gene also reduces plasmid retention. Because RacA is only expressed during sporulation, however, another factor would have to be responsible for maintaining plasmids during vegetative growth.

AlfA forms bundles in vivo and in vitro, and this behavior likely plays a role in plasmid segregation. Although the interaction appears to be driven by electrostatics, we observed AlfA bundles in salt concentrations as high as 2M KCl (figure 1D), suggesting that the bundling observed in vivo occurs by the same mechanism as the spontaneous lateral association we observed in vitro. We do not know the precise role of bundling in plasmid segregation but there are several attractive possibilities. First, by providing high local concentrations of filaments, bundles can stabilize weak interactions with accessory proteins. In addition, spontaneous

bundling may gather all AlfA filaments in the cytoplasm into a single, DNA-segregating structure. By restricting movement of filaments, such a structure could provide a positional “memory” that persists beyond the lifetime of an individual filament. In other words, a filament bundle could act as a stable template, guiding the treadmilling or sliding of individual plasmid-attached filaments.

The unique architecture of the AlfA filament demonstrates a remarkable diversity within the actin family. While we think of filament formation as the ‘function’ of an actin-like protein, the residues that mediate filament formation are not highly conserved. The most highly conserved sequences in the actin family line the nucleotide binding pocket. Residues that mediate subunit-subunit contacts in the filament are quite divergent. This divergence leads to remarkable differences in filament architecture. To date, structures have been determined for four actin family filaments: conventional actin (35) MreB (10) ParM (28) and now, AlfA. While all of them can be described as two-stranded filaments, the relationship between the strands is different in each case. In one (actin) the strands form a right-handed helix; in two (ParM and AlfA) the helix is left-handed; and one (MreB) lacks helical twist altogether. Furthermore, even though ParM and AlfA both form left-handed helices, the symmetry of the two filaments is quite different as is the orientation of subunits with respect to the filament axis, with the ATP binding cleft of AlfA rotated roughly 45° relative to its orientation in the other filaments (figure 7). In that regard, a similar orientation of the ATP binding cleft was observed in a ‘ribbon’ model, based on crystal contacts from the structure of the b-actin-profilin complex (31) The Schutt model suggested that actin (and actin-like) monomers can be assembled into polymers with significantly different architectures and subsequent studies of bacterial actins have borne this

out.

The divergence in the subunit-subunit contact sites in the family of actin filaments indicates one of three things: 1) the architectural constraints of filament formation are loose enough to permit significant genetic drift; 2) there is positive evolutionary pressure on the bacterial actin-like proteins to produce filaments with divergent architecture; and 3) filament formation evolved multiple times in the actin family.

ACKNOWLEDGEMENTS

We thank members of the Mullins and Vale labs for discussions and support, J.Pogliano (UCSD) for providing plasmids, E. H. Egelman (UVA) for discussions on the structure of ParM, and M. Braunfeld, S. Zheng, and E. Branlund (UCSF) for technical assistance.

This work was supported by grants to R.D.M from the Sandler Family Supporting Foundation the National Institutes of Health (R01-GM079556). J.P. is supported by an N.S.F. predoctoral fellowship.

REFERENCES

1. **Becker E., N. C. Herrera, F. Q. Gunderson, A. I. Derman, A. L. Dance, J. Sims, R. A. Larsen, and J. Pogliano**. 2006. DNA segregation by the bacterial actin AlfA during Bacillus subtilis growth and development. EMBO J **25**:5919-31.

2. **Ben-Yehuda S., D. Z. Rudner, and R. Losick**. 2003. RacA, a Bacterial Protein That Anchors Chromosomes to the Cell Poles. Science **299**:532-536.

3. **Blanchoin L., and T. D. Pollard**. 2002. Hydrolysis of ATP by polymerized actin depends on the bound divalent cation but not profilin. Biochemistry **41**:597-602.

4. **Campbell C. S., and R. D. Mullins**. 2007. In vivo visualization of type II plasmid segregation: bacterial actin filaments pushing plasmids. J Cell Biol **179**:1059-66.

5. **Carballido-López R.** 2006. The bacterial actin-like cytoskeleton. Microbiol Mol Biol Rev **70**:888-909.

6. **Dayel M. J., E. A. Holleran, and R. D. Mullins**. 2001. Arp2/3 complex requires hydrolyzable ATP for nucleation of new actin filaments. Proc. Natl. Acad. Sci. U.S.A **98**:14871-14876.

7. **Earl A. M., R. Losick, and R. Kolter**. 2007. Bacillus subtilis Genome Diversity. J. Bacteriol. **189**:1163-1170.

8. **Egelman E. H.** 2000. A robust algorithm for the reconstruction of helical filaments using single-particle methods. Ultramicroscopy **85**:225-234.

9. **Egelman E. H.** 2007. The iterative helical real space reconstruction method: surmounting the problems posed by real polymers. J. Struct. Biol **157**:83-94.

10. **van den Ent F., L. A. Amos, and J. Löwe**. 2001. Prokaryotic origin of the actin cytoskeleton. Nature **413**:39-44.

11. **van den Ent F., J. Møller-Jensen, L. A. Amos, K. Gerdes, and J. Löwe**. 2002. F-actin-like filaments formed by plasmid segregation protein ParM. EMBO J **21**:6935-6943.

12. **Flyvbjerg H., E. Jobs, and S. Leibler**. 1996. Kinetics of self-assembling microtubules: an "inverse problem" in biochemistry. Proc. Natl. Acad. Sci. U.S.A **93**:5975-5979.

13. **Frank J., M. Radermacher, P. Penczek, J. Zhu, Y. Li, M. Ladjadj, and A. Leith**. 1996. SPIDER and WEB: processing and visualization of images in 3D electron microscopy and related fields. J. Struct. Biol **116**:190-199.

14. **Garner E. C., C. S. Campbell, and R. D. Mullins**. 2004. Dynamic instability in a DNA-segregating prokaryotic actin homolog. Science **306**:1021-5.

15. **Garner E. C., C. S. Campbell, D. B. Weibel, and R. D. Mullins**. 2007. Reconstitution of DNA segregation driven by assembly of a prokaryotic actin homolog. Science **315**:1270-1274.

16. **Holmes K. C., D. Popp, W. Gebhard, and W. Kabsch**. 1990. Atomic model of the actin filament. Nature **347**:44-49.

17. **Holy T. E., and S. Leibler**. 1994. Dynamic instability of microtubules as an efficient way to search in space. Proc. Natl. Acad. Sci. U.S.A **91**:5682-5685.

18. **Jensen R. B., and K. Gerdes**. 1997. Partitioning of plasmid R1. The ParM protein exhibits ATPase activity and interacts with the centromere-like ParR-parC complex. J. Mol. Biol **269**:505-513.

19. **Jones L. J., R. Carballido-López, and J. Errington**. 2001. Control of cell shape in bacteria: helical, actin-like filaments in Bacillus subtilis. Cell **104**:913-922.

20. **Kawamura M., and K. Maruyama**. 1970. Polymorphism of F-actin. I. Three forms of paracrystals. J. Biochem **68**:885-899.

21. **Komeili A., Z. Li, D. K. Newman, and G. J. Jensen**. 2006. Magnetosomes are cell membrane invaginations organized by the actin-like protein MamK. Science **311**:242-245.

22. **Korn E. D., M. F. Carlier, and D. Pantaloni**. 1987. Actin polymerization and ATP hydrolysis. Science **238**:638-644.

23. **Ludtke S. J., P. R. Baldwin, and W. Chiu**. 1999. EMAN: semiautomated software for high-resolution single-particle reconstructions. J. Struct. Biol **128**:82-97.

24. **Mayer J. A., and K. J. Amann**. 2009. Assembly properties of the Bacillus subtilis actin, MreB. Cell Motil. Cytoskeleton **66**:109-118.

25. **Mindell J. A., and N. Grigorieff**. 2003. Accurate determination of local defocus and specimen tilt in electron microscopy. J. Struct. Biol **142**:334-347.

26. **Møller-Jensen J., R. B. Jensen, J. Löwe, and K. Gerdes**. 2002. Prokaryotic DNA segregation by an actin-like filament. EMBO J **21**:3119-3127.

27. **Nishida E., and H. Sakai**. 1983. Kinetic analysis of actin polymerization. J. Biochem **93**:1011-1020.

28. **Orlova A., E. C. Garner, V. E. Galkin, J. Heuser, R. D. Mullins, and E. H. Egelman**. 2007. The structure of bacterial ParM filaments. Nat. Struct. Mol. Biol **14**:921-926.

29. **Orlova A., A. Shvetsov, V. E. Galkin, D. S. Kudryashov, P. A. Rubenstein, E. H. Egelman, and E. Reisler**. 2004. Actin-destabilizing factors disrupt filaments by means of a time reversal of polymerization. Proc. Natl. Acad. Sci. U.S.A **101**:17664-17668.

30. **Pettersen E. F., T. D. Goddard, C. C. Huang, G. S. Couch, D. M. Greenblatt, E. C. Meng, and T. E. Ferrin**. 2004. UCSF Chimera--a visualization system for exploratory research and analysis. J Comput Chem **25**:1605-1612.

31. **Schutt C. E., J. C. Myslik, M. D. Rozycki, N. C. Goonesekere, and U. Lindberg**. 1993. The structure of crystalline profilin-beta-actin. Nature **365**:810-816.

32. **Sept D., and J. A. McCammon**. 2001. Thermodynamics and kinetics of actin filament nucleation. Biophys. J **81**:667-674.

33. **Srivatsan A., Y. Han, J. Peng, A. K. Tehranchi, R. Gibbs, J. D. Wang, and R. Chen**. 2008. High-Precision, Whole-Genome Sequencing of Laboratory Strains Facilitates Genetic Studies. PLoS Genet **4**:e1000139.

34. **Tanaka T., and M. Ogura**. 1998. A novel Bacillus natto plasmid pLS32 capable of replication in Bacillus subtilis. FEBS Letters **422**:243-246.

35. **Trinick J., J. Cooper, J. Seymour, and E. H. Egelman**. 1986. Cryo-electron microscopy and three-dimensional reconstruction of actin filaments. J Microsc **141**:349-360.

36. **Wu L. J., and J. Errington**. 2003. RacA and the Soj-Spo0J system combine to effect polar chromosome segregation in sporulating Bacillus subtilis. Molecular Microbiology **49**:1463-1475.

TABLES AND FIGURES

0.1M KCl

	Pelleting	Light Scattering
ATP	**2.4 uM** +/- 0.6 (n = 4)	**2.7 uM** +/- 0.2 (n = 3)
ADP	**10.1 uM** +/- 3.1 (n = 6)	
AMPPNP	**1.8 uM** +/- 0.02 (n = 2)	
GTP	**2.0 uM** +/- 0.8 (n = 4)	**3.4 uM** +/- 0.3 (n = 3)
GDP	**19.5 uM** +/- 2.2 (n = 5)	

1.8M KCl

	Pelleting	Light Scattering
ATP	**4.3 uM** +/- 0.6 (n = 3)	**6.1 uM** +/- 1.3 (n = 4)
ADP	**33.8 uM** (n = 1)	
GTP	**7.9 uM** +/- 4.1 (n = 2)	**>8uM** (n = 1)
GDP	**47.1 uM** (n = 1)	

Table 1. **Critical concentrations of AlfA assembly.**

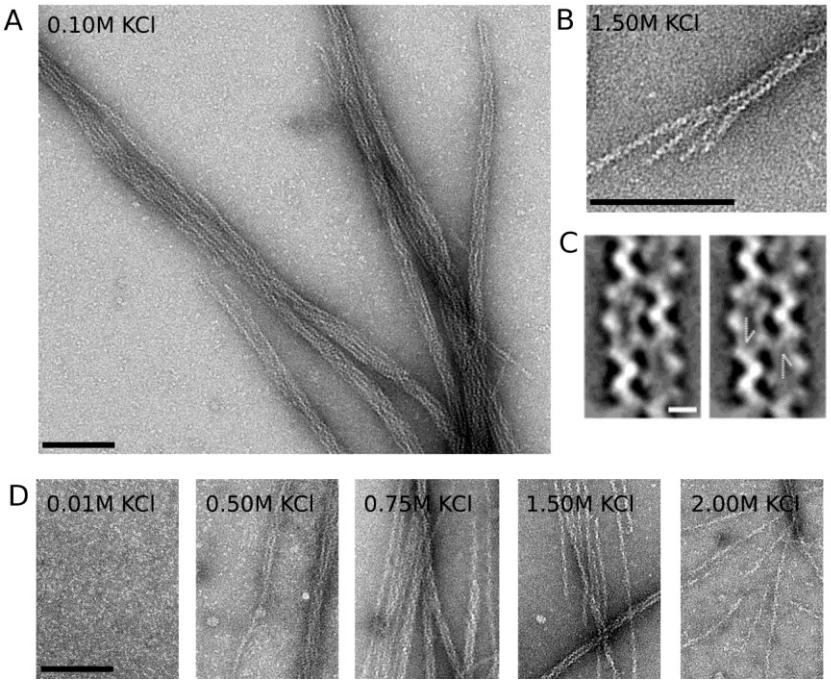

Figure 1. **AlfA polymerizes into filaments that spontaneously associate into mixed-polarity bundles.** (A) AlfA filament bundles formed in the presence of Mg2+ and ATP, and in the absence of crowding agents. 5µM AlfA was polymerized with 5mM ATP, stained with 0.75% uranyl formate and visualized by transmission electron microscopy. Similar bundles are observed in GTP. (Conditions: 100mM KCl, 25mM Tris HCl pH 7.5, 1mM MgCl, 1mM DTT, 25º C). (B) Splayed ends show that bundles are composed of individual filaments. (C) One of four reference-free class averages from a 102-segment data set of filament pairs, showing that filaments can associate with one another in an antiparallel fashion. The arrows in the image at right highlight the antiparallel features. White scale bar, 10nM. (D) Bundles can be disassociated under high salt concentrations, with single filaments predominating at 2.00M KCl. Black scale bars, 100nm.

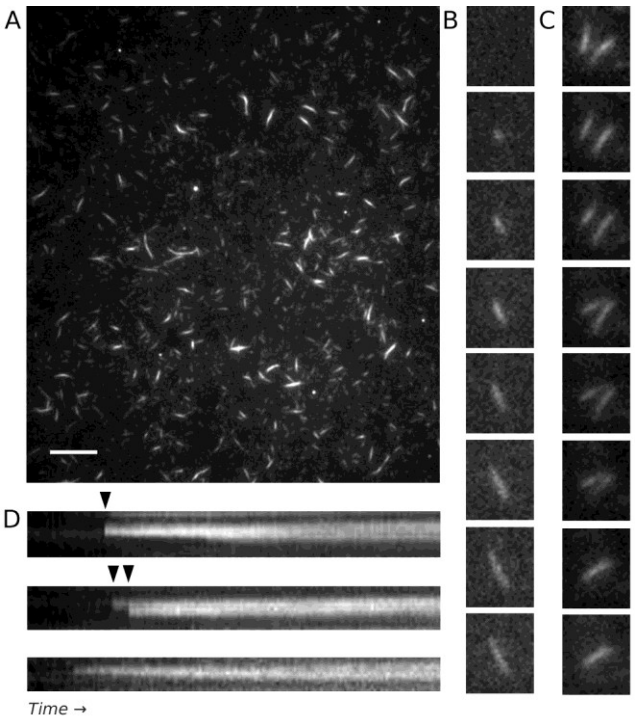

Figure 2. **AlfA filament and bundle assembly observed by TIRF microscopy: bundles show no evidence of dynamic instability.** (A) TIRF microscopy of a field of Cy3- and biotin- labeled 3µM AlfA five minutes after polymerization reveals stable filamentous structures of varying fluorescence intensity. The variation in intensity is consistent with filament bundles. Scale bar, 10µm. (Conditions: 20% Cy3 labeled, 5% biotin labeled AlfA (3uM total) with 5mM ATP in buffer as in Figure 1A). (B) Bundles appear to elongate bidirectionaly, but polarity of the filaments (and the directionality of their elongation) cannot be determined. Time interval, 40 seconds. (Conditions: as above, with addition of 0.5% BSA) (C) Observation of an annealing event between two bundles adhered to the coverslip. Time interval, 7 seconds. (Conditions: as in A). (D) Kymographs collected immediately after addition of nucleotide show that bundles can grow by lateral annealing events (arrows). Time scale, 2.5 minutes. (Conditions: as in A).

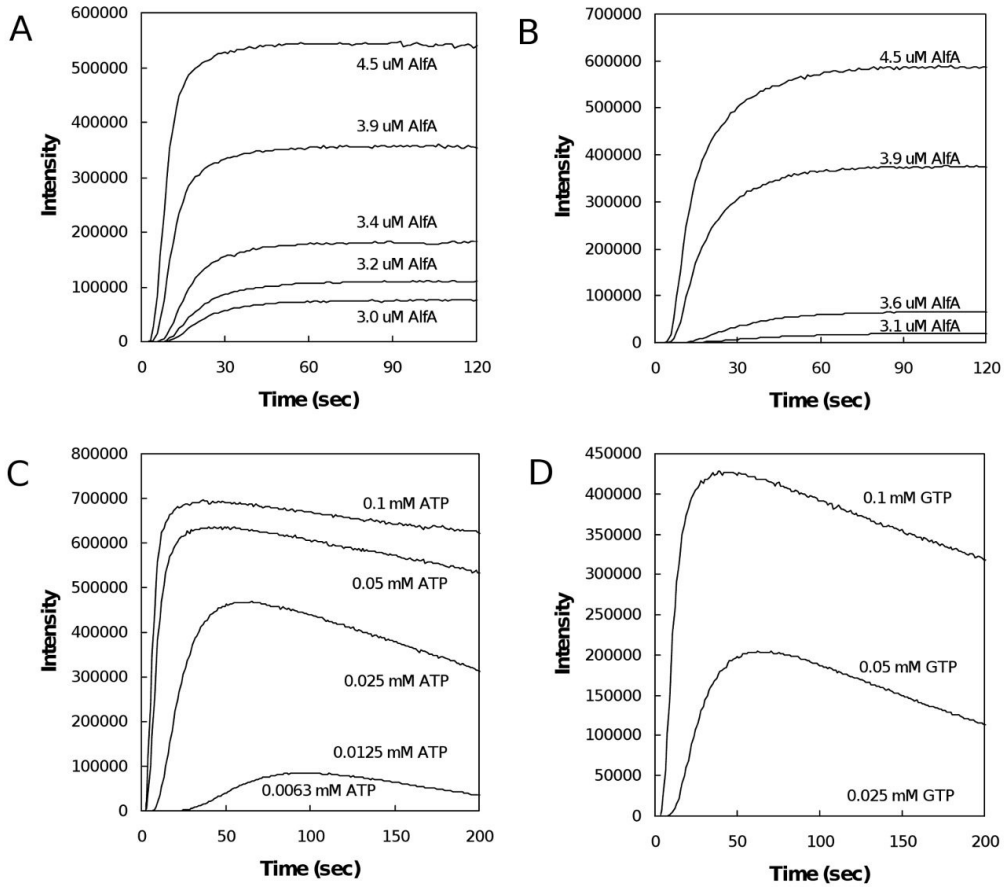

Figure 3. **Light scattering.** (A-B) Assembly of filaments in saturating levels (5mM) of ATP (A) and GTP (B) is similar (Conditions: as in Figure 1A). (C-D) 4.7µM AlfA does not rapidly depolymerize in low levels of either ATP (C) or GTP (D), providing evidence for a lack of dynamic instability. AlfA appears to be less stable in GTP. (Conditions: as above.)

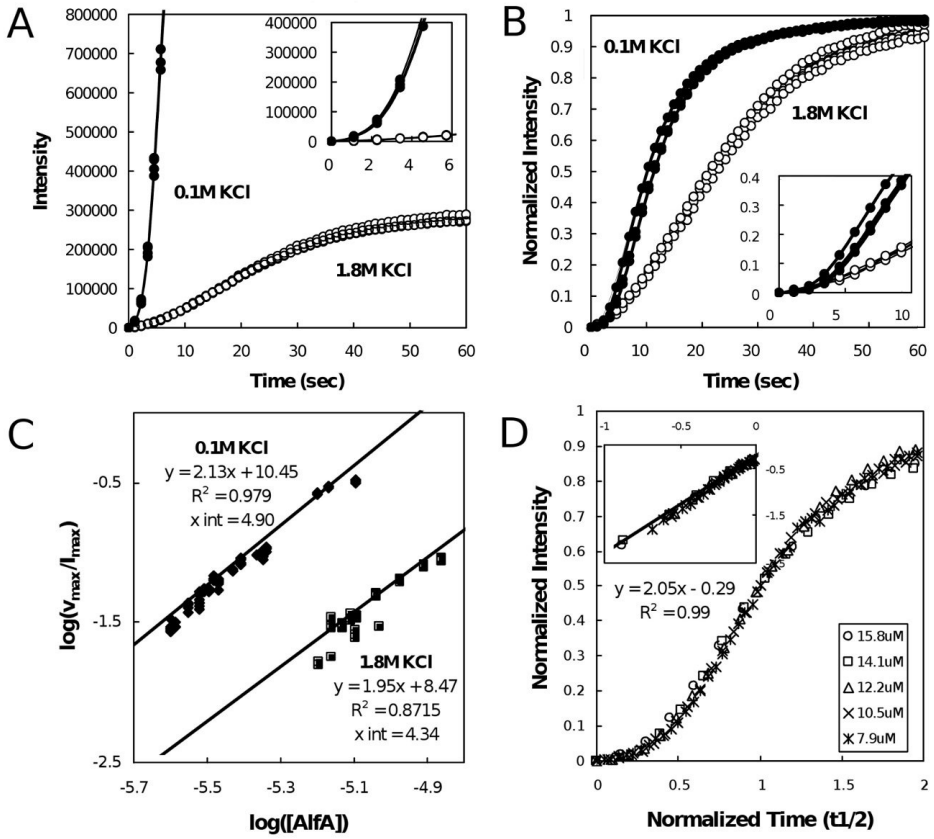

Figure 4. **Light scattering in high salt.** (A-B) Assembly of filaments in 5mM ATP in 0.1M KCl (filled circles) is more rapid than in 1.8M KCl (hollow circles). (A) At identical instrument settings, assembly of 3.8µM AlfA in 0.1M KCl quickly saturates the detector, while the signal from 7.4µM AlfA in 1.8M KCl remains modest. Both concentrations are approximately 1uM above the critical concentrations for the relevant KCl concentration. Inset, early time points. (Conditions otherwise as in figure 3A). (B) Intensity-normalized traces taken at similar instrument settings show that polymerization is slower in 1.8M KCl (Conditions as in A, except that 0.1M KCl runs are at 3.1µM AlfA). (C) Determination of nucleus size and relative nucleation rates for AlfA in high and low salt. To generate a data point, the maximal velocity of a light scattering trace was divided by the maximal intensity of the signal, and the log of this value plotted against the log of AlfA concentration. The slopes of the regression lines are proportional to n/2, where n is the

number of monomers required to form a nucleus. This analysis suggests that AlfA assembles with a nucleus size of four monomers in both 0.1M KCl and 1.8M KCl, but its nucleation is approximately 10 times faster in low salt. (D) Data collapse of light scattering traces taken at 1.8M KCl using varying concentrations of AlfA after normalization of maximum intensities and half times. Inset, log-log plot of the same data, showing that the slope of a regression line equals 2. (Conditions: as in A.)

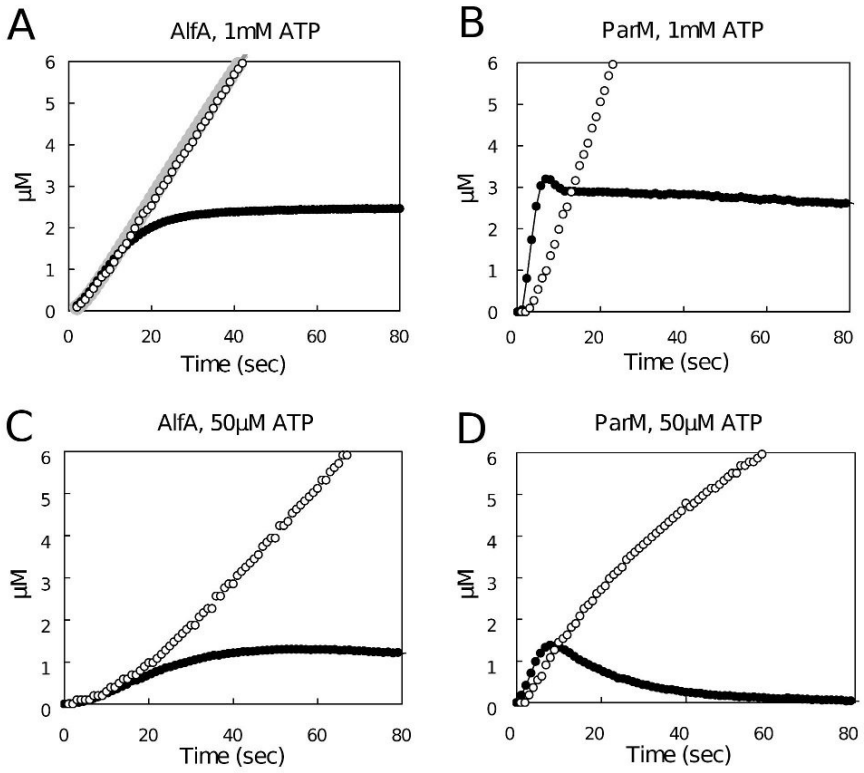

Figure 5. **Phopshate release assays.** (A) Phosphate release ([Pi] measured by colorimetric assay, hollow circles) and polymer formed ([polymeric AlfA] measured by light scattering, filled circles) by 8.6µM AlfA in 1mM ATP and 1.8M KCl, with conditions otherwise as in figure 1A. The gray line represents [Pi] release predicted by our model. (B) Phosphate release and polymer formed

by 4.9µM ParM in 0.1M KCl and 1mM ATP, with conditions otherwise as in (A). (C) Phosphate release and polymer formed by 8.6µM AlfA in 50µM ATP, with conditions otherwise as in (A). (D) Phosphate release and polymer formed by 4.9µM ParM in 50uM ATP, with conditions otherwise as in (B).

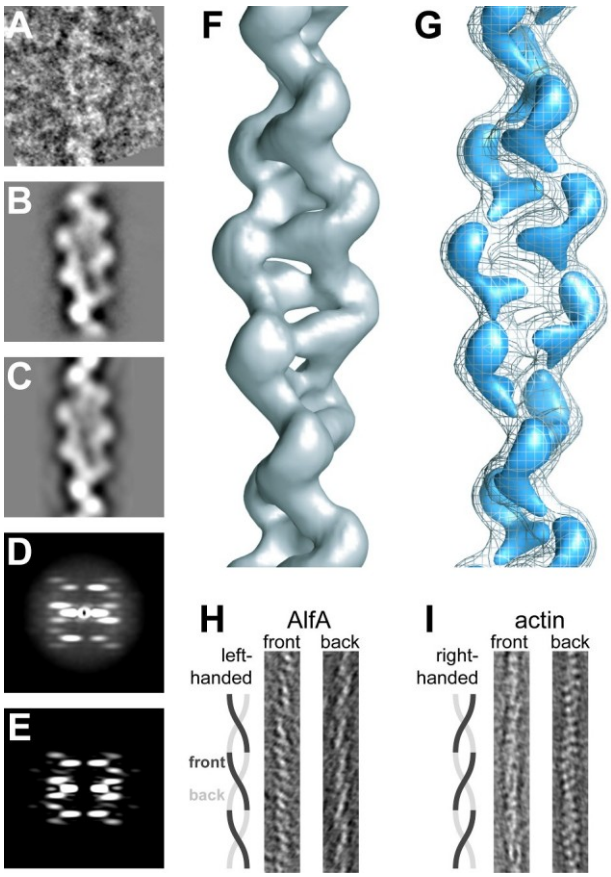

Figure 6. **Three-dimensional reconstruction of single AlfA filaments.** (A) A representative segment of AlfA filament from negative stain micrographs (Conditions: 1.25M KCl, 25mM Tris HCl pH 7.5, 1mM MgCl, 1mM DTT, 25º C, 5mM AMPPNP, 7µm AlfA). (B) Average of 757 AlfA segments after iterative helical real space reconstruction. (C) Reprojection of the final AlfA filament model in the same orientation as the average in B. Scalebar, 5 nm. (D) Average power

spectrum of 2000 non-overlapping segments. (E) The two-dimensional power spectrum of the final AlfA filament model is very similar to the average power spectrum in D. (F) The three-dimensional reconstruction of an AlfA filament, contoured to enclose the expected mass the AlfA subunits. (G) The AlfA filament at the same countour as F (mesh) and at a higher contour level (blue) which clearly shows the separation between the two strands of the filament and between AlfA subunits in each strand. (H) Approximately 3.5 nm slices from a tomographic reconstruction of a single AlfA filament demonstrate that the long pitch of the helix is left-handed. (I) A tomogram of actin, prepared in the same manner as for AlfA in H as a control, demonstrates the well-established right-handed pitch of the long helix. In H and I the width of the image is 25 nm.

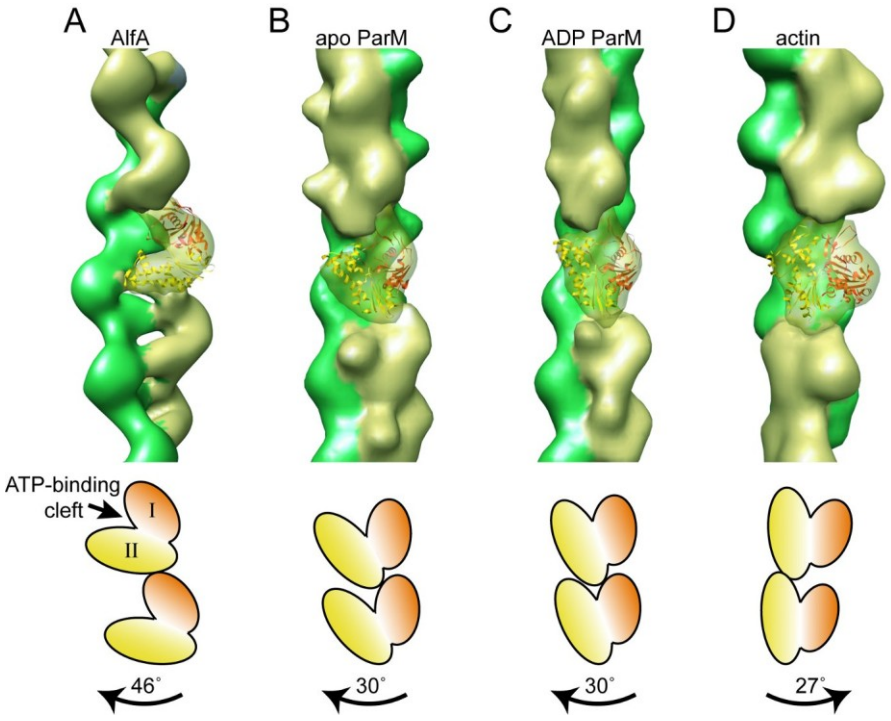

Figure 7. **The architecture of the AlfA filament is distinct from both ParM and actin.** (A) The reconstruction of the AlfA filament, with each strand represented in a different color. A single

subunit of the filament has been rendered transparent, with the crystal structure of apo ParM manually fit into the density. The crystal structure is colored orange in domain I and yellow in domain II. B-D) For comparison, simulated EM density calculated from models of the ParM filament in the apo and ADP-bound conformations (Egelman, E.H., personal communication) and actin filaments(29) are shown in the same color scheme. The cartoons at bottom indicate the orientation of subunits in the filament; the magnitude and direction of the rotation between subunits moving up each strand is indicated with arrows.

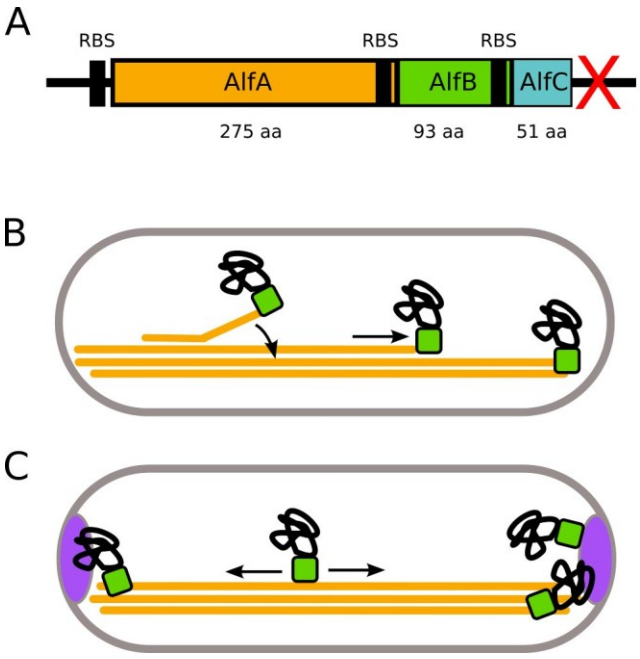

Figure 8. **Hypothetical mechanisms for plasmid segregation by a bundling polymer lacking dynamic instability.** (A) Diagram of the *alf* operon, showing relative sizes and positions of open reading frames and their ribosome binding sites. Red "X" indicates a transcriptional terminator. (B) "End interaction." Plasmids, through an adapter protein (perhaps AlfB), can bind to the ends of individual filaments. The ends are either encountered randomly by diffusion or created through the nucleation of a new filament, which would soon anneal to the existing bundle

(curved arrow). Plasmids track with the growing end (straight arrow) until they reach one of the cell poles, where they are likely to remain because of the high concentration of filament ends. With some frequency, plasmids will be transmitted to the other pole by tracking with the end of a new filament. (C) “Lateral interaction.” Plasmids bind filaments laterally, and can travel with treadmilling or sliding filaments. If a plasmid reaches the cell pole, it is maintained there by another factor (such as RacA).

Table 1. **Critical concentrations for AlfA in high and low salt.** Critical concentrations were determined as described in Materials and Methods.

SUPPLEMENTAL FIGURES

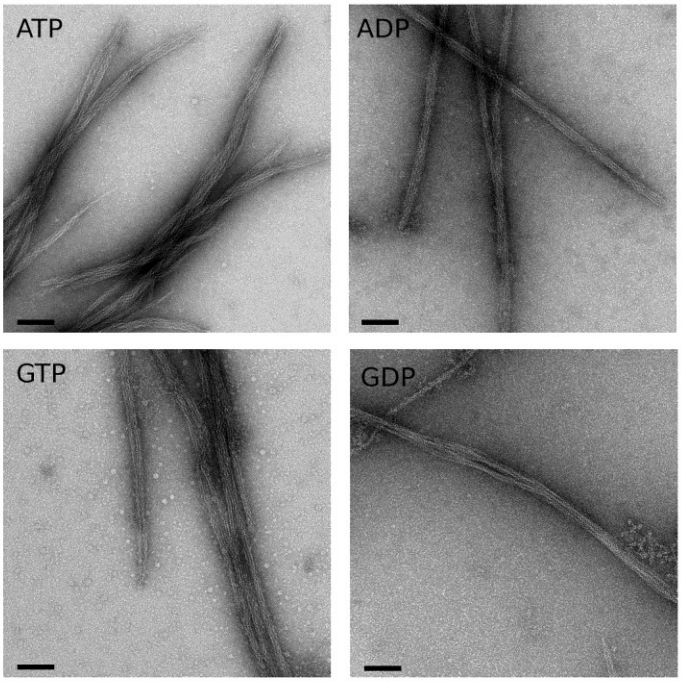

Supplemental figure 1. **AlfA assembly can occur in various nucleotides**. 15µM AlfA was polymerized with 5mM of nucleotide in 0.1M KCl polymerization buffer at 25º, stained with 0.75% uranyl formate, and visualized by transmission electron microscopy. Scale bar, 100nm.

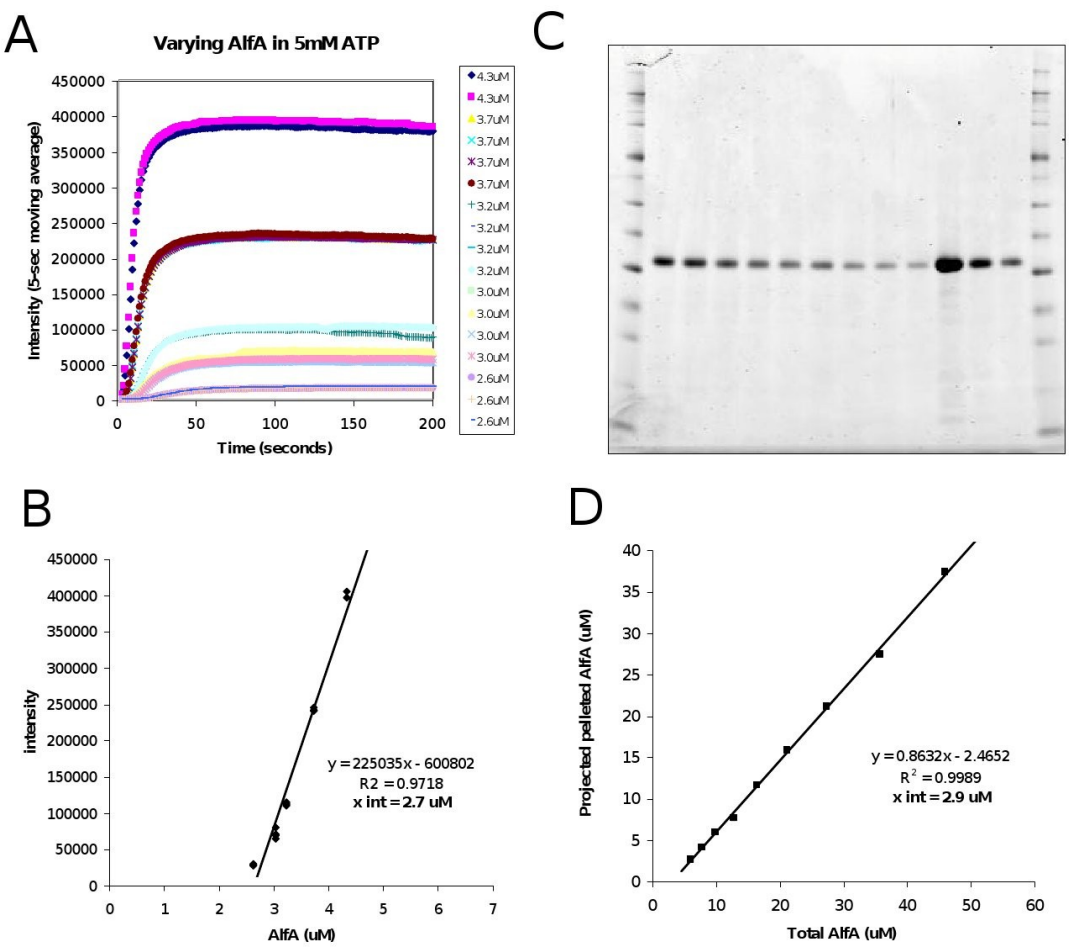

Supplemental figure 2. **Determination of critical concentration by light scattering and pelleting.** (A) Sample light scattering traces from an experiment with varying concentrations of AlfA in 0.1M KCl polymerization buffer and 5mM ATP at 25˚ C, after smoothing by moving average with an interval of 5 seconds. (B) Maximum intensities of light scattering traces from panel A plotted against AlfA concentration. The x-intercept of a linear fit provides the critical concentration. (C) Sample gel showing supernatants from a high-speed pelleting assay in conditions identical to panel A, with AlfA concentrations ranging from 45µM to 4.5µM. The last three lanes are nucleotide-free controls used to calibrate the gel. (D) The material depleted from the supernatant in the presence of ATP (taken as [total] – [supernatant]) is plotted against the total

protein concentration in the reaction. The x-intercept of a linear fit provides the critical concentration.

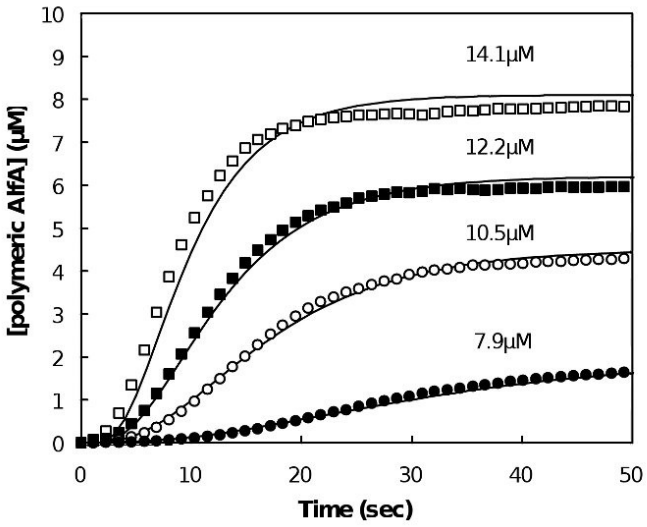

Supplemental figure 3. **Data collapse of light scattering curves.** Light scattering traces of varying concentrations of AlfA taken in 1.8M KCl polymerization buffer with 5mM ATP at 25˚ C. All traces were normalized to their maximum intensities, calculated as the maximum of a 5-second moving average of the original trace. All traces were also normalized to their half time, calculated as the time at which the half-maximum intensity was reached. The overlap of all curves suggests that the same mechanism governs assembly at varying AlfA concentrations.

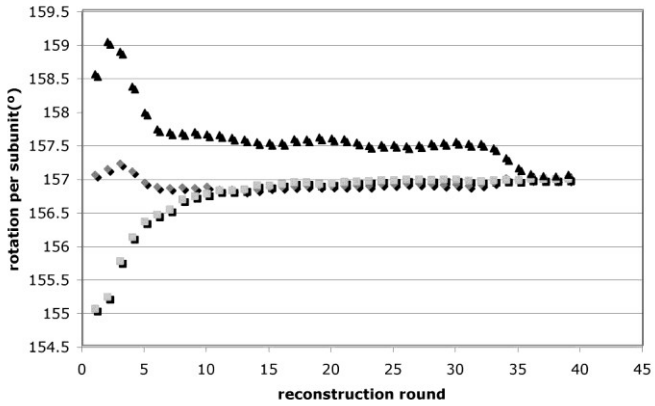

Supplemental figure 4. **The helical symmetry parameters of AlfA filaments converge to the same rotation per subunit from different initial symmetry parameters.** Independent reconstructions were carried out using a cylinder as the initial model in all cases and starting at three different initial symmetries: 155º, 157º and 158.5º. In each case, the rotation per subunit refined to 157º. The initial plateau at 157.5º in the upper trace may reflect the existence of a subpopuation of segments with this rotation.

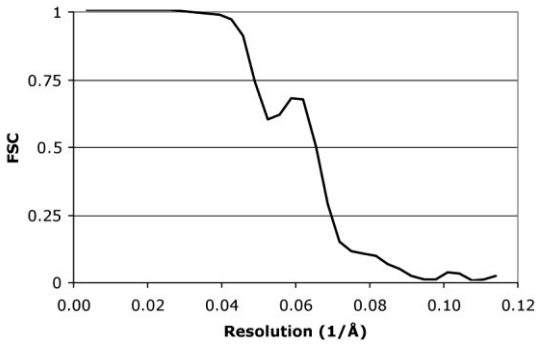

Supplemental figure 5. **The apparent resolution of the AlfA filament reconstruction is ~15 Å by the FSC 0.5 criterion.** Two separate volumes were calculated, each from half the total data set divided by filament, to ensure that no overlapping segments are used in the separate

reconstructions. The dip in the FSC value around 19 Å is likely due to the limited range of defocus values used in the reconstruction – the average defocus used was 1.1 μm, corresponding to a first zero in the CTF at about 19 Å.

Chapter 3: Effect of AlfA on plasmid position, maintenance and mobility

Introduction

The initial characterization of AlfA (Becker 2006) suggested that AlfA provided a segregation benefit to plasmids both during vegetative growth and sporulation. However, especially in light of our earlier findings (Polka 2009) that AlfA was kinetically and structurally divergent from other actins previously identified, we sought to understand whether the mechanism of segregation was likewise unique.

We imaged several modalities for AlfA to use in interacting with plasmids: first, it might provide a one-dimensional track to allow plasmids to diffuse along; second, it could push plasmids with polymerization like a formin riding the end of an actin filament; third, it could pull plasmids like a kinetochore on the end of an anaphase microtubule; and fourth, the ends of the filament could act as special binding sites for plasmids.

Additional constraints would allow non-random segregation to emerge from these simple mechanisms. For example, if a limited number of plasmids could stably bind to each end of a filament or filament bundle, any excess plasmids would find occupancy only at the other end of the cell. A second possibility is that the pulling or pushing mechanism could, by mechanically joining one plasmid to another, non-randomly move plasmids in opposite directions.

To discriminate among these possibilities, both the simple models for how plasmids interact with filaments, and the complex ones regarding how these interactions lead to spatial organization, we developed strains and plasmids for fluorescence visualization of AlfA *in vivo* and used bulk plasmid maintenance assays to measure the efficiency of various mutants.

Construction of strains

We adapted an integrating plasmid carrying CFP-lacI under the control of the pxyl promoter (Derman 2008) by replacing the CFP with GFP and mcherry. This plasmid was integrated into the chromosome of PY79 or swrA+ *B. subtilis.* This lacI bound to a lacO array cloned into miniplasmids containing an *E.coli* origin and ampicillin resistance marker as well as a *B. subtilis* tetracycline resistance marker. The miniplasmid also contained the origin region from pLS32, with *alf* versions also containing the *alf* operon.

To express fluorescently tagged AlfA, all well-characterized inducible promoter systems (xyl, tet, lac) were already exhausted by the strain and plasmid. Therefore I cloned a second, GFP-tagged copy of AlfA at the end of the *alf* operon.

Table 1. **Plasmids used in this study**.

Name	**Genotype**	**Backbone**	**Purpose**
Mini	pLS32 origin	--	Control plasmid for plasmid maintenance assay
Mini + lacO	As above with lacO array	Mini	Control plasmid for visualization of plasmids
Mini + alf	As mini with Alf operon region	Mini	Plasmid maintenance assay
Mini + alf + alfA-GFP	Second copy of AlfA	Mini + alf	Visualization of filaments
Mini + alf + alfA-mEOS	Second copy of AlfA	Mini + alf	Visualization of filaments for STORM and photoconversion

Mini + alf + alfA-GFP + lacO	lacO array	Mini + alf + GFP	Visualization of plasmid and filaments
Mini + alf nonbundling	KK21AA, KK101AA mutagenesis of AlfA	Mini + alf	Effect of bundling on portioning
Mini + alf – AlfC	Stop codon insterted into AlfC	Mini + alf	Effect of AlfC on partitioning

Table 2. **Strains used in this study**.

Name	**Genotype**	**Purpose**
PY79	General lab strain	Plasmid maintenance assay
swrA+	Nonchaining	Plasmid maintenance assay
PY79 mCherry-lacI	General lab strain + pxyl lacI	Visualization of filaments and plasmids
PY79 GFP-lacI	General lab strain + pxyl lacI	Visualization of plasmids only
swrA+ mCherry-lacI	Nonchaining + pxyl lacI	Visualization of filaments and plasmids
swrA+ GFP-lacI	Nonchaining + pxyl lacI	Visualization of plasmids only

***Bacillus subtilis* live cell imaging**

Adopting a method from Joe Pogliano's lab, 1% Seakem agarose was dissolved in 0.25X LB or CH media. FM4-64 was used at 1:5000 to visualized membranes. The agarose was cast into a deep well concavity slide covered with a normal slide to ensure a smooth surface. Air holes

were then cut out of the pad, leaving an approximately 8mm channel in the middle onto which cells were spread and covered with a No. 1.5 coverslip. Cells were imaged at 25 or 30 degrees.

Plasmid position

We used swrA+ cells, which infrequently chain, so that cell boundaries can be detected by their brightfield signals. These images were segmented and the fluorescence signals from the plasmids detected with MicrobeTracker (Sliusarenko, 2011). By looking analyzing the position of plasmids along the long axis of the cell, we generated histograms of plasmid position in various cases (figure 1). However, while AlfA may subtly enhance the number of plasmids positioned closer to the poles in the two-foci cells, there is no dramatic difference among all four cases, suggesting that the Alf system does not efficiently maintain plasmids at specific places in the cell.

To further study this subtle apparent difference in the placement of plasmid in two-foci cells, we calculated the distance between these two foci relative to the cell length, plotting the frequency of this spacing as a normalized histogram (figure 2). This data is necessarily limited by the fact that two plasmids very close to one another, at least beneath the Nyquist limit, cannot be distinguished from one focus. Furthermore, the data cannot explain the efficiency of the AlfA segregation system as measured by plasmid maintenance assays in solution, perhaps due to artifacts arising from the imaging setup, and the fact that the actual average copy number is more likely to be 4-6 per cell (Tanaka 1998). Nevertheless, any two plasmids which are spaced more than half of the cell length apart from one another will by default be equally segregated to daughter cells, and the plasmids carrying the *alf* operon show an increase in this fraction. This indicates that the *alf* operon exerts an effect on whole populations of cells, increasing the spacing of pairs of plasmids.

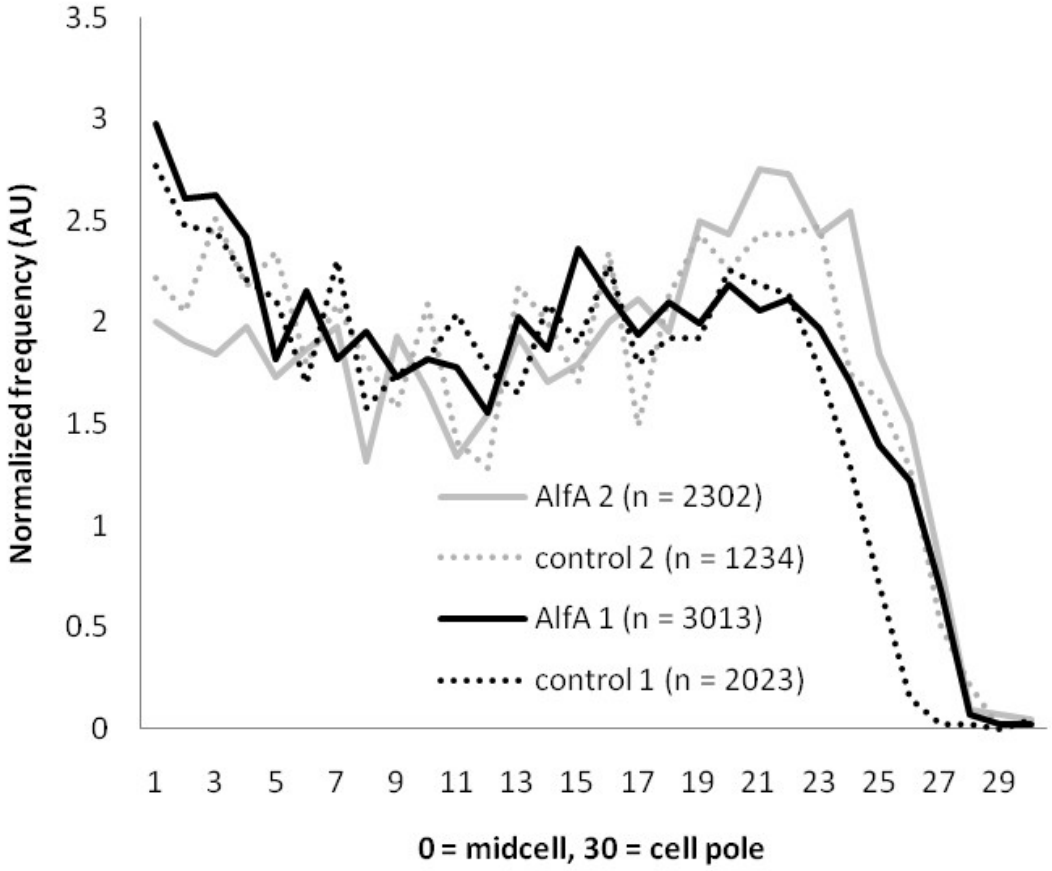

Figure 1. **Position of plasmids along the long axis of the cell in the presence and absence of the *alf* operon.** Single time point images of cells were sorted based on the number of plasmid foci in the fluorescence channel detected within the segmented boundary in brightfield. The positions of these plasmids were calculated relative to the length of the cell. In this histogram of normalized frequency of plasmid position, the midcell is represented at the origin of the horizontal axis, and the pole in the 30th bin of the histogram.

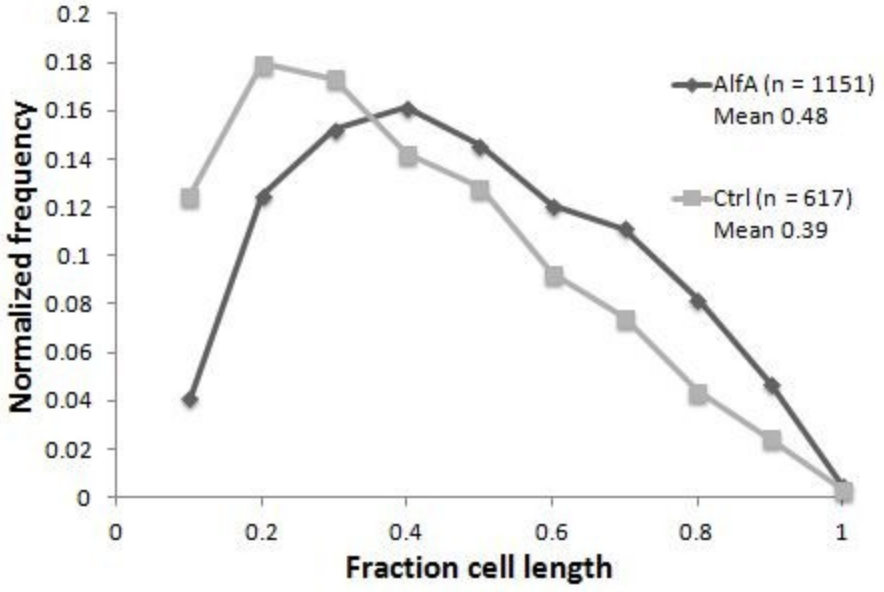

Figure 2. **Distance between plasmids in cells with exactly two foci.** The distance between foci in the 2-plasmid cells from figure 1 was calculated and normalized to the length of the cells. No two plasmids are positioned at 0 (as this would indicate that the plasmids are visually indistinguishable) and plasmids at 1 would be exactly at opposite poles of the cell.

Plasmid tracking

Plasmids under the influence of cytoskeletal elements may experience different mobilties within the cell. For example, ParM increases the ballistic motion of plasmids (Campbell 2007) while ParA makes plasmids appear more confined (Derman 2008). The presence of a mobility effect on AlfA-containing plasmids might not only suggest an interaction with a cytoskeletal element, but also suggest information about the nature of that element. To quantify the motion of these plasmids, we obtained time-lapse movies of plasmid foci. Using the U-Track suite (Jaqaman 2008) we first identified the foci in each individual frame with Gaussian fitting, and then constructed tracks by linking these foci from one time point to the next based on a maximum likelihood matrix. Parameters were chosen based on minimization of clearly

spurious track joining events, visible by eye in projections such as figure 3b. The same parameters were used for control and *alf*-containing plasmids.

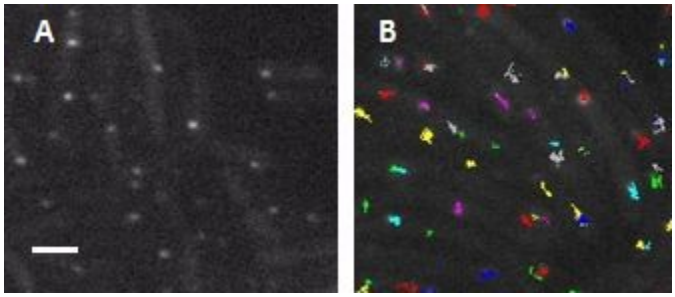

Figure 3. **Labeled plasmids and superimposed tracks.** GFP-lacI was expressed under the control of a xylose promoter from the chromosome. LacI bound to a lacO array carried on plasmids, creating foci (A) tracked using U-Track (Jaqaman 2008), creating trajectories overlaid on a similar image in various colors (B). Scale bar, 2um.

Mean squared displacement analysis

We then used these plasmid trajectories to calculate mean squared displacement (MSD) relationships for each track over varying time intervals (tau). The scaling of the MSD over increasing intervals reveals the character of an object's motion (confined, diffusive, or ballistic), which can be most easily appreciated by fitting a power function to the data and calculating the α factor, or scaling exponent. Because of the nature of DNA and the bacterial cytoplasm, plasmids under no outside mechanical influence are expected to have an α of 0.4 (Weber 2010). Indeed, we found a very similar α for the averaged tracks from our control plasmids (figure 4). The AlfA plasmids, however, had a higher α of approximately 0.73. This suggests that there is a an additional ballistic component to this motion. Interestingly, the coefficient of this power function is decreased in the case of *alf* plasmids.

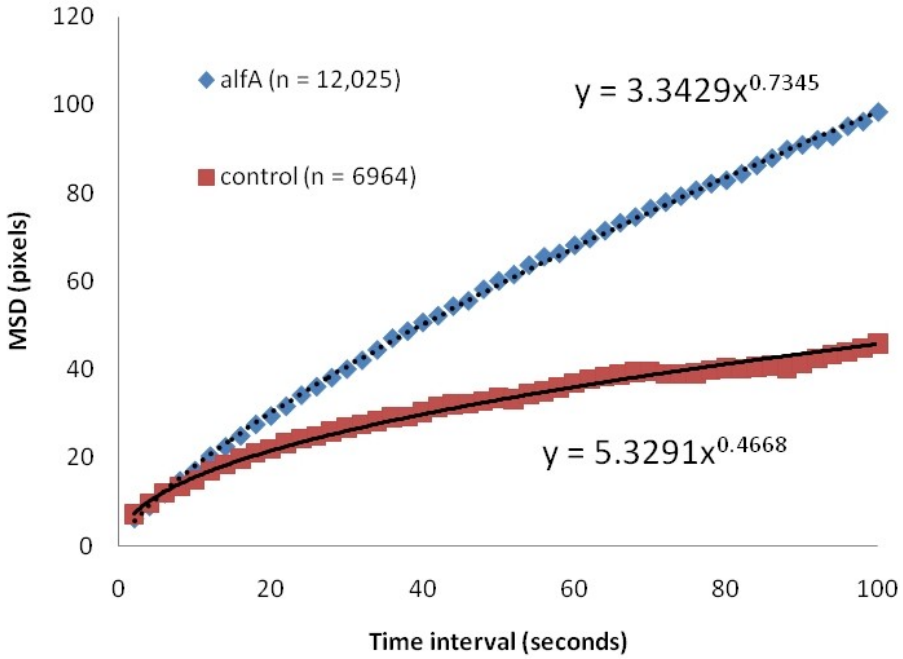

Figure 4. **MSD plots of plasmids containing and lacking *alf*.** Plasmid trajectories from movies of SwrA+ cells containing GFP-lacI and either a control miniplasmid or an *alf* miniplasmid were analyzed to calculate the MSD over tau (time interval). The α factor, represented as the exponent of the fit, is approximately 0.47 in the case of control plasmids, but 0.73 in the case of *alf* containing plasmids.

Detecting transient directed motions (speed correlation index, instantaneous MSD)

We subjectively compared of the motions of plasmids in the presence of AlfA versus those with no *alf* operon. The AlfA plasmids appear to undergo short bursts of directed motion, even though their mobility appears to be overall somewhat restricted. To determine if this phenomenon is the result of observer bias, we developed software tools to pick out short bursts of directed motion from a mostly diffusive track. We adapted the Speed Correlation Index (Bouzigues 2007), which correlates the angle of velocity between different time points. An

object moving perfectly ballistically will have an SCI of 1, while an object that moves randomly will have an SCI of 0. We also calculated the alpha factor of an "instantaneous" MSD, that is, we found the sliding MSD for short (~5 frame) windows of longer tracks. We used the later method to identify ballistic ($\alpha > 1.8$) tracks in plasmid tracking data (Figure X)

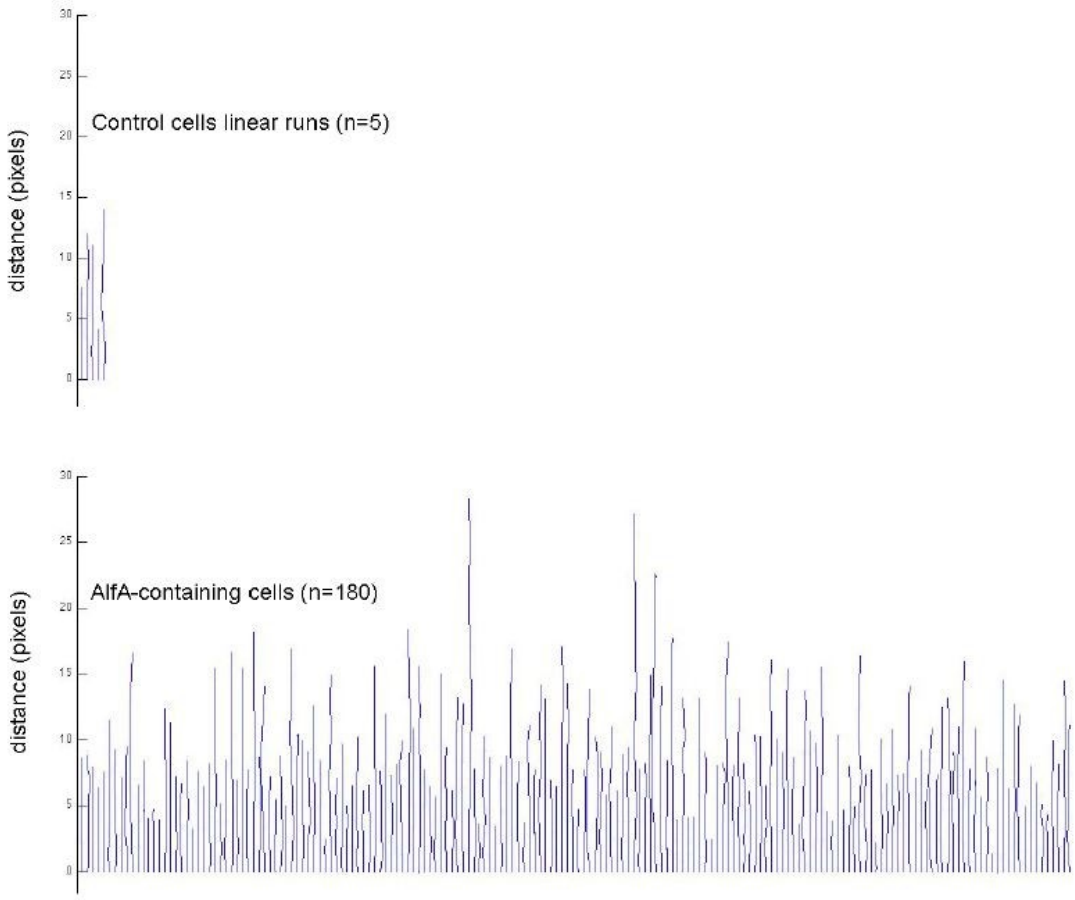

Figure 5. **Linear tracks of plasmid motion identified with instantaneous MSD analysis.** Identified ballistic ($\alpha > 1.8$) segments of tracks were rotated along the vertical axis and plotted next to one another to demonstrate that the algorithm is successful in pulling out highly directed motions from 16,000 control tracks and 30,000 AlfA tracks. Notably, these motions, even normalized for the difference in size of the datasets, are much more frequent in the presence of *alf*.

Visualization of AlfA and plasmids

We made timelapse movies of AlfA (visualized by a second, GFP-tagged copy of AlfA cloned into the *alf* operon) and plasmids (carrying lacO arrays which bind to mCherry-lacI expressed from the chromosome). In many of these cases, the noise floor in the filament image was too high to reliably distinguish filaments, indicated that there is a large pool of monomers of short filaments not involved in the clear bundles which can sometimes be visualized (red channel in figure 6). Nevertheless, we were able to observe transient ballistic motions of plasmids that correlated with changes in the AlfA signal. Namely, plasmids moved along tracks defined by existing filaments, and also followed the growing ends of filaments (Figure 6A). Furthermore, foci moving apart from one another were often accompanied by a filament growing between them (Figure 6B).

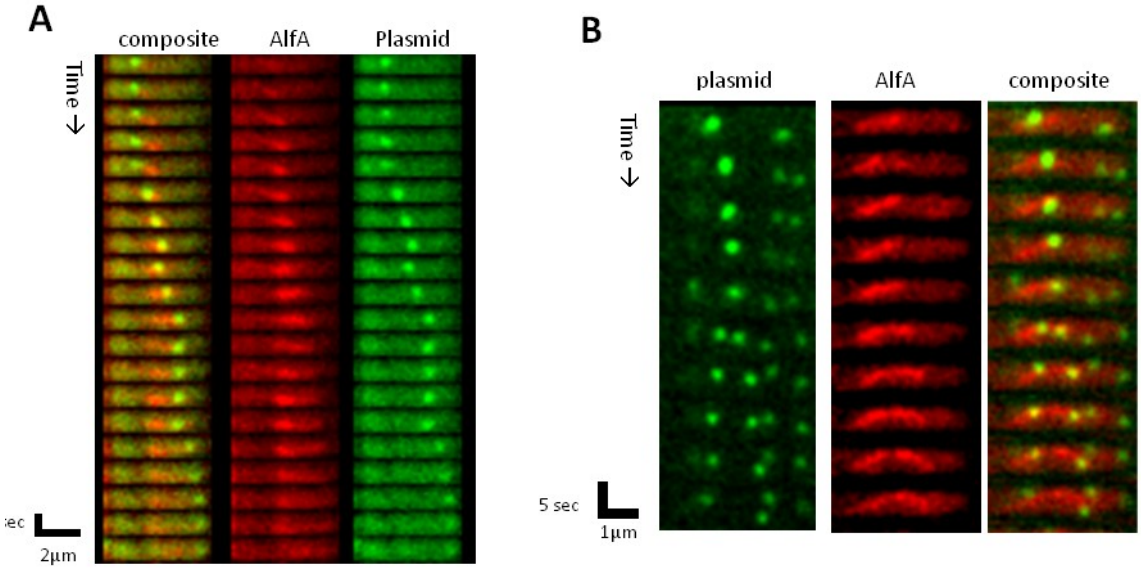

Figure 6. **Correlation of AlfA and plasmid movements.** Timelapse microscopy of a single B. subtilis cell expressing a chromosomal mCherry-lacI (green) decorating plasmids bearing a lacO

array and carrying the *alf* operon with a GFP tagged second copy of the AlfA gene (red). Plasmid foci move along existing AlfA filaments (A, first 5 frames) and also track the growing end of filaments (remainder of frames). Foci can also be segregated from one another (B) by the polymerization of AlfA between them.

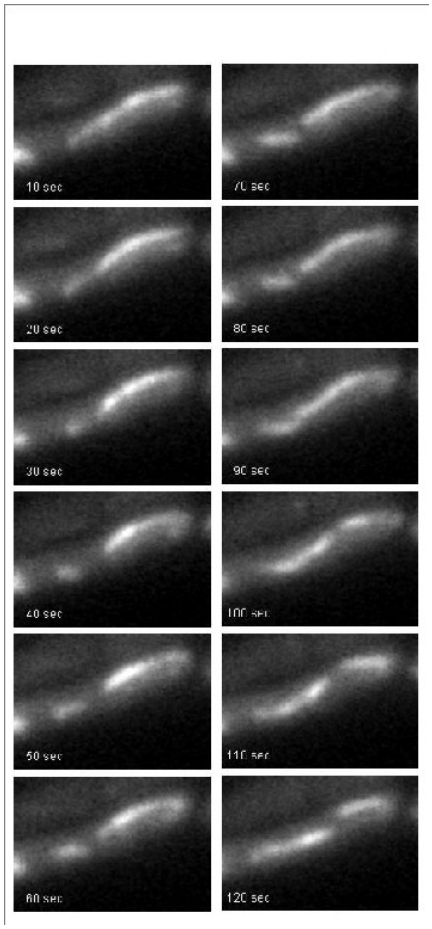

Figure 7. **AlfA filaments undergo complex remodeling behaviors.** In this montage of cells carrying a second copy of GFP-labeled AlfA, a filamentous structure visible in the first frame (10 seconds) breaks into smaller pieces which can independently rotate (40 seconds). Later, the signal from these pieces overlaps again, and a second break occurs (100 seconds). These behaviors are reminiscent of the lateral annealing seen in vitro in Chapter 2. Time interval, 10 seconds.

Nonbundling mutant

The filament remodeling behaviors observed in figure 7, reminiscent of bundling interactions we saw *in vitro*, suggested that existing AlfA filaments may bundle together *in vitro*. This interaction could potentially mechanically link one plasmid to another, and thus might be important for building a segregating spindle. To test this hypothesis, we generated a mutant (figure 8) which has markedly reduced bundling activity. This mutant can be efficiently purified, though it has a slightly higher apparent critical concentration than the wild type AlfA (approximately 4uM vs. 2.4uM).

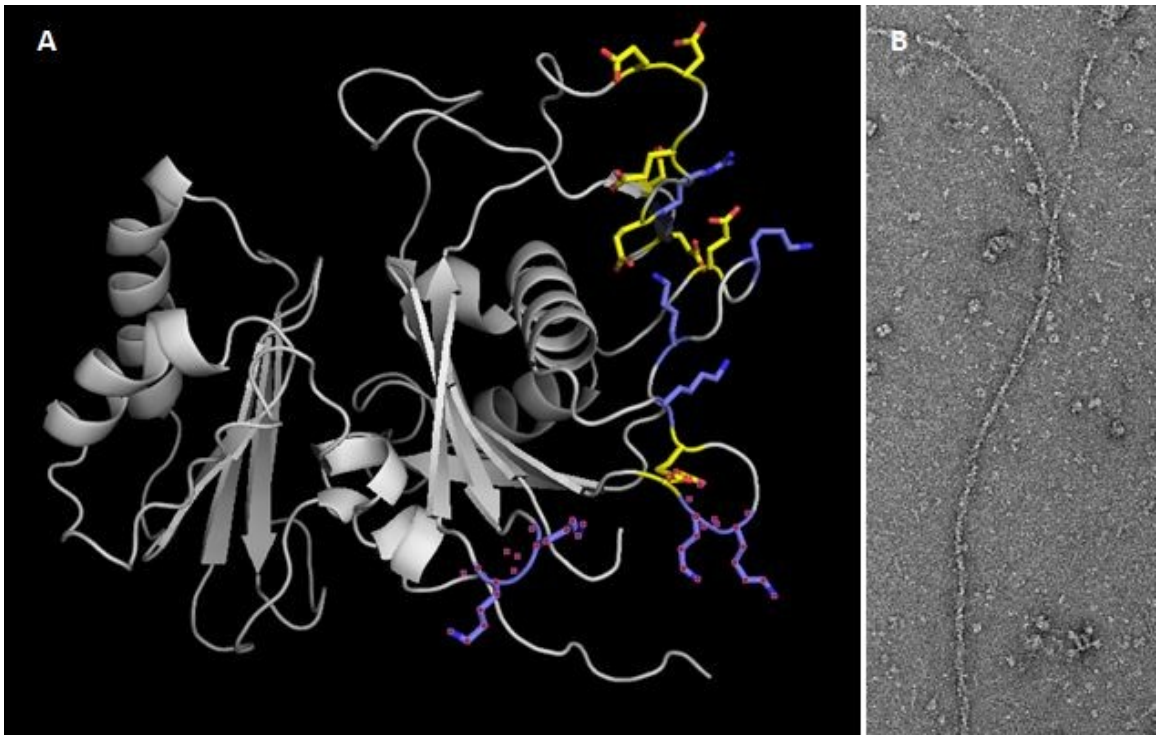

Figure 8. **Design of the non-bundling mutant.** A homology model (A) constructed using the ParM crystal structure (van den Ent, 2002) by Justin Kollman revealed several charged residues likely to fall on the outside of a filament, based on a helical reconstruction from EM (Polka

2009). Four lysine residues, highlighted above with red dots, were mutated to alanines (K21A, K22A, K101A, K102A) to produce a mutant which, by negative stain EM, can be observed to form single filaments in 95% of structures (B).

Plasmid maintenance assay

To determine whether bundling mutant was defective for plasmid segregation *in vivo*, we performed a plasmid maintenance assay based on techniques used in the Pogliano lab (Becker 2006), using an exponential decay to model the loss of plasmids over subsequent generations. We found that AlfA reduces plasmid loss by 10-fold each generation when compared to control plasmids (table 3). Our strain containing the second, fluorescent copy of AlfA conferred only a 4-fold advantage, with a similar effect observed for the mutant deficient in bundling.

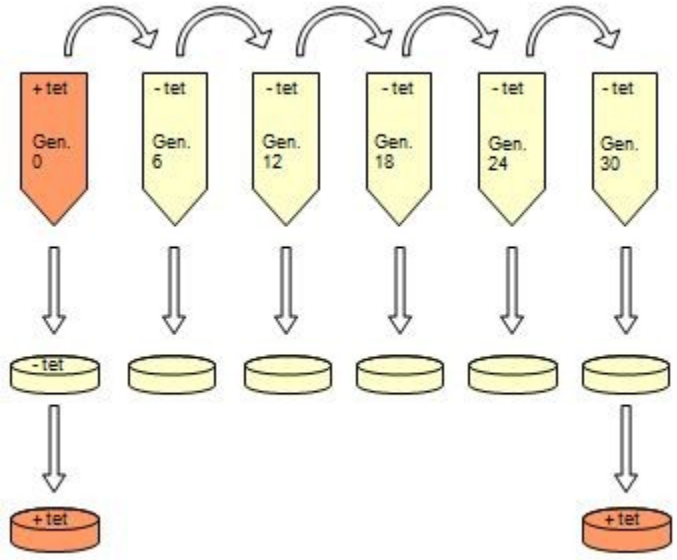

Figure 9. **Schematic of the plasmid maintenance assay.** Cells containing an antibiotic-resistance bearing plasmid are grown to early exponential phase (A600 = 0.2 – 0.4) under selection. This

culture is plated to non-selective media at a density that will produce single colonies (100ul of 10^{-4}) and diluted at 1:64 into non-selective media. Every 6 generations, when the A600 again reaches 0.2-0.4, the dilution process is repeated for as many generations as time allows. The colonies which grow up on the non-selective media the following day are individually streaked to selective media to determine the fraction of cells at each time point which carried the plasmid.

Table 3. **Plasmid loss rates.**

Genotype of miniplasmid	**Loss rate/generation**	**n**
origin only	6.06%	2
+ alf	0.59%	5
+ alf w/2nd AlfA-GFP or EOS	1.35%	2
+ KK21DD,KK101DD alf	1.47%	1

Discussion

Our plasmid maintenance data confirm literature reports of AlfA as a stability determinant (Becker 2006), though our exponential model for plasmid loss better approximates effect of the *alf* system than the previously published linear model. Our findings regarding the effect of this system on plasmid position suggested that AlfA effected this segregation benefit by increasing the spacing between pairs of plasmids, not by positioning them specifically in the cell. Our mobility data strongly suggested that AlfA filaments actively move plasmids, and the direct observation of filaments and plasmids together argued that plasmids are pushed by growing filaments.

This leads to a model whereby filaments provide the motive force for segregation. However, how can filaments move plasmids in relation to one another, preferentially separating them rather than pulling them together, or moving them randomly about the cell? There must be some mechanism for mechanically joining plasmid-bound filaments to one another. Given the behaviors of AlfA filaments, it is possible that such a joining could be mediated by the same lateral bundling which we observed annealing preexisting filaments in TIRF (chapter 2). This model would predict that a non-bundling mutant would be severely defective in plasmid segregation, perhaps able to increase the mobility of plasmids because AlfA polymerization would be largely unaffected, but unable to correlate the movement of one plasmid to another through mechanical coupling. However, while the mutant we generated efficiently reduces bundling *in vitro*, it has a relatively modest effect on segregation efficiency *in vivo.* This may be due to penetrance of the mutant – for example, the cytoplasm is a crowded environment that may promote bundling, even with a reduction in surface charge.

References

1. Becker, E. *et al.* DNA segregation by the bacterial actin AlfA during Bacillus subtilis growth and development. *EMBO J* **25**, 5919–31 (2006).

2. Bouzigues, C. & Dahan, M. Transient Directed Motions of GABAA Receptors in Growth Cones Detected by a Speed Correlation Index. *Biophysical Journal* **92**, 654–660 (2007).

3. Derman, A. I., Lim-Fong, G. & Pogliano, J. Intracellular mobility of plasmid DNA is limited by the ParA family of partitioning systems. *Mol. Microbiol* **67**, 935–946 (2008).

4. Jaqaman, K. *et al.* Robust single particle tracking in live cell time-lapse sequences. *Nat Methods* **5**, 695–702 (2008).

5. Polka, J. K., Kollman, J. M., Agard, D. A. & Mullins, R. D. The Structure and Assembly Dynamics of Plasmid Actin AlfA Imply a Novel Mechanism of DNA Segregation. *J. Bacteriol.* **191**, 6219–6230 (2009).

6. Sliusarenko, O., Heinritz, J., Emonet, T. & Jacobs-Wagner, C. High-throughput, subpixel precision analysis of bacterial morphogenesis and intracellular spatio-temporal dynamics. *Mol. Microbiol.* **80**, 612–627 (2011).

7. Tanaka, T. & Ogura, M. A novel Bacillus natto plasmid pLS32 capable of replication in Bacillus subtilis. *FEBS Letters* **422**, 243–246 (1998).

8. van den Ent, F., Møller-Jensen, J., Amos, L. A., Gerdes, K. & Löwe, J. F-actin-like filaments formed by plasmid segregation protein ParM. *EMBO J* **21**, 6935–6943 (2002).

9. Weber, S. C., Spakowitz, A. J. & Theriot, J. A. Bacterial chromosomal loci move subdiffusively through a viscoelastic cytoplasm. *Phys. Rev. Lett.* **104**, 238102 (2010).

Chapter 4: DNA binding and modulation of AlfA assembly by AlfB

Introduction

Many questions remain unanswered by the *in vivo* studies presented in chapter 3. Though AlfA polymerization appears to push plasmids, and the system appears to space plasmids further apart from one another r, there is no indication of how filament assembly is controlled, how the plasmids interact with the filaments, or how the filaments turn over and remodel. Crucially to developing a model for how non-random DNA distribution emerges, the *in vivo* data does not explain how plasmids become mechanically coupled to one another, especially in light of the modest segregation defect presented by the non-bundling mutant. Does filament assembly or elongation happen specifically in the presence of two plasmids, or are preexisting plasmid-bound structure able to capture one another with bundling? If filament assembly does change in the presence of plasmids, how is assembly elsewhere suppressed, when our preliminary *in vitro* characterization (chapter 2) suggests that AlfA is stable on its own?

To address these questions, we sought to study the effects of other operon components on the kinetics of AlfA assembly and its filament structure. We began with AlfB, the DNA-binding protein directly downstream of AlfA, and then included the DNA sequence to which it binds, *parN* (Tanaka, 2010).

Purification of AlfB

We cloned a codon-optimized version of AlfB into a pETM11 vector, containing an N-terminal His10 tag followed by a TEV recognition site. After binding the high-speed supernatant to a HiTrap columns charged with cobalt resin, we cleaved the elution with TEV protease,

running the solution back over the column to remove the free His tag. Following gel filtration over a Supderdex 200 column, we dialyzed the protein into 20% glycerol to freeze.

In order to determine the ratio of AlfA to AlfB to give a sense of how much AlfB should be used *in vitro*¸ we raised antibodies to purified AlfA and AlfB in New Zealand white rabbits, blotting extracts from identical optical densities of *B. subtilis* with antisera. The bands produced from Alexa488 secondary antibody staining were scanned and imaged with a Typhoon, their intensity compared to bands resulting from known concentrations of purified AlfA and AlfB. This analysis revealed that the ratio of AlfA to AlfB was approximately 1:3 (data not shown).

However, copelleting assays suggest that a small fraction of the purified AlfB, between 10-15%, is competent to bind AlfA (data not shown). Thus, a 2-fold excess of AlfB to AlfA probably most likely approximates the effect of this protein *in vivo*.

Binding of AlfB to DNA

Tanaka reported that AlfB binds specifically to a region of DNA surrounding the promoter of the *alf* operon, which he termed *parN.* This region is comprised of 3 degenerate repeats of 8bp (Tanaka 2010). Addition of a 120-bp region containing these repeats specifically produced flexible complexes visible by negative stain EM (figure 1), which do not appear to have a consistent curvature like ParR complexes decorating *parC* DNA.

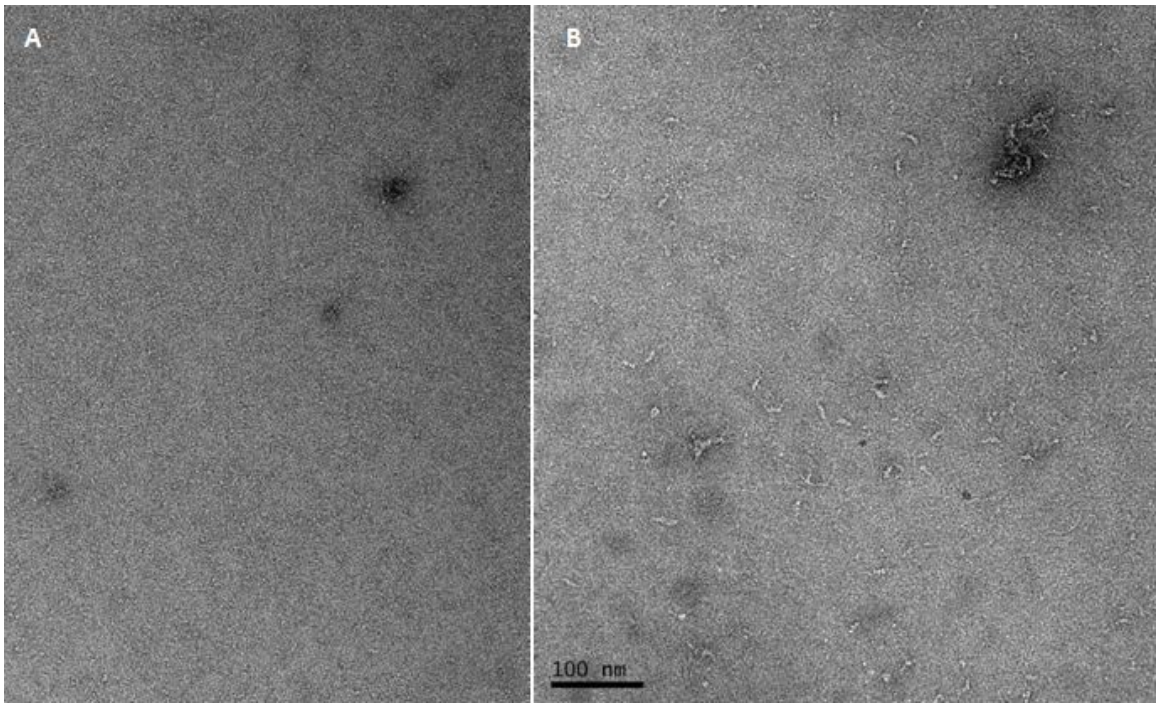

Figure 1. **EM of negatively stained AlfB-ParN complexes**. 1uM AlfB was mixed with either 50nM ParC DNA (360bp) from the *par* operon as a control (A) or with 50nM ParN from the *alf* operon in polymerization buffer (100mM KCl, 25mM Tris pH 7.5, 1mM MgCl2, 1mM DTT) and incubated for 10 minutes before staining with 0.75% uranyl formate.

Effect of AlfB on AlfA assembly with and without DNA

To study the interaction of AlfA and AlfB, we first need to have an estimate of the relative concentration of these proteins *in vivo* so as to conduct *in vitro* experiments in a physiological regime. To do this, we ordered antisera from New Zealand White Rabbits injected with purified AlfA and AlfB from Pacific Immunology. We found that the relative concentration of AlfB : AlfA is roughly 1 : 1.9 (figure 2). This is a relatively large concentration, much higher than what would be necessary for binding to *parN* repeats in DNA.

AlfB appears to have a complex interaction with AlfA. As noted above, AlfB does copellet with AlfA polymer, indicating that it is competent to bind to filaments. It also, however,

seems to increase the critical concentration of assembly (figure 3C). Though this effect appears modest, if the active % of AlfB is taken into account, 5uM AlfB is actually only approximately 0.5uM active AlfB, and this is very close (0.4uM) to the change in AlfA critical concentration that is effected, indicating that perhaps AlfA is able to sequester monomers.

AlfB likely does not depolymerize existing AlfA filaments, however. Watching polymer disassembly in the presence and absence of AlfB (figure 3B and A, respectively) does not reveal any changes in the relative off-rates. However, there is a very dramatic change in the light scattering signal (figure 3) when AlfB is added. The light scattering signal of bundles of AlfA is dominated by the effect of bundling (chapter 2). AlfB addition is likely not inducing depolymerization (based on figure 3), and may be a result of sequestering some monomers, but is more likely a result of changing the form of the polymer by reducing bundling (figure 5). Interestingly, the loss of light scattering intensity is recovered by the addition of DNA, but this DNA must specifically contain the *parN* sequence (figure 5). Some of this effect may come from sequestering AlfB onto the DNA. In this reaction there is roughly 500nM active AlfB and only about 20nM of DNA. Because *parN* consists of 3 degenerate repeats, each of these may bind a dimer of AlfB, meaning that perhaps one-third of the AlfB is involved in DNA binding. However, the recovery of the light scattering signal is absolute, suggesting that the DNA is also changing the form of the polymer by encouraging bundling.

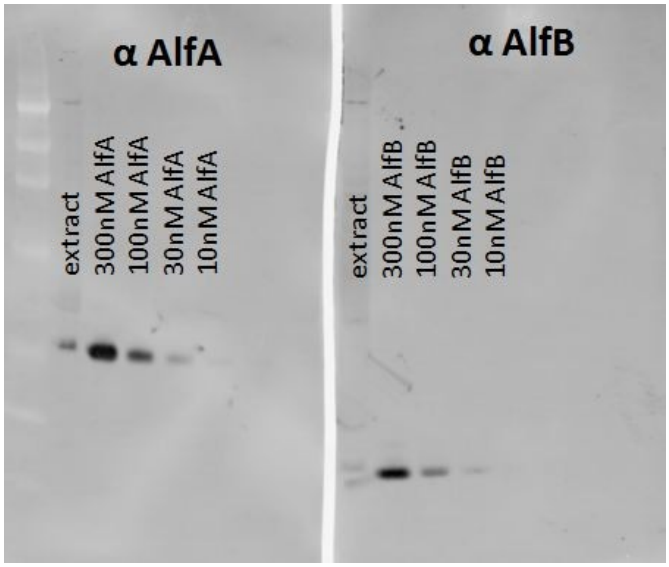

Figure 2. **Western blot of AlfA and AlfB from equal volumes of *B. subtilis* extract**. Anti-rabbit, Alexa488 conjugated secondary antibodies were visualized with a Typhoon scanner and band intensities quantified with ImageJ. The protein standards following each extract band were then used to estimate the relative concentration of proteins in the loaded extract, revealing a ratio of AlfB to AlfA of approximately 1 to 1.9.

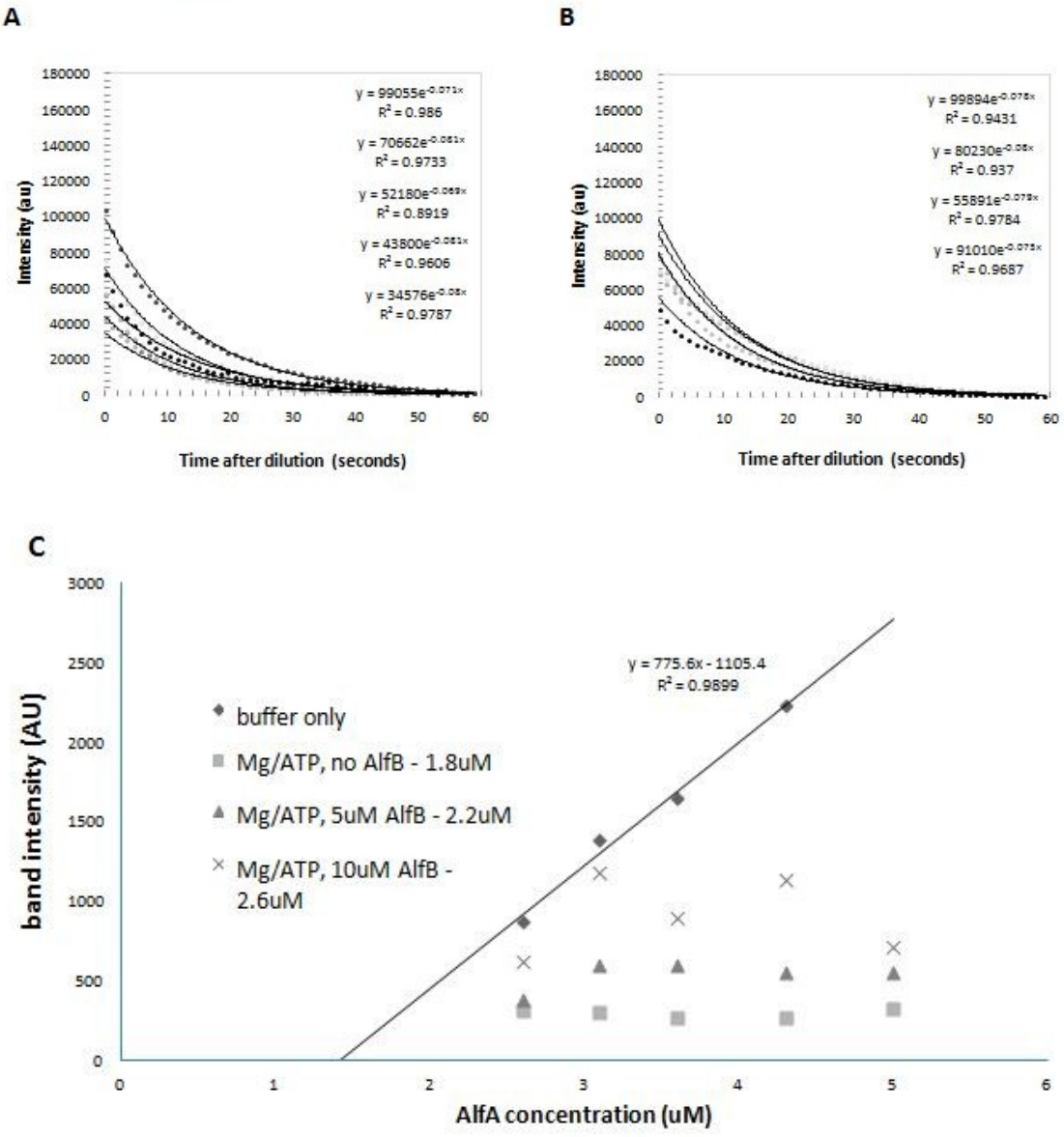

Figure 3. **AlfB modestly affects AlfA critical concentration, but does not promote depolymerization.** 4uM AlfA was rapidly diluted to 2uM, below the critical concentration, in a fluorimeter measuring the intensity of the right-angle light scattering signal at 320nm to monitor depolymerization of polymer. In the absence of B, the decay of the signal can be fit with a function (A) that is not significantly different from that which can be fit when AlfB is added to the diluting buffer for a final concentration of 2uM (B), indicating that AlfB does not dramatically increase the off-rate. To determine if AlfB modifies the critical concentration of polymerization

(C), AlfA at varying concentrations was polymerized with 5mM Mg/ATP (squares), 5mM Mg/ATP and 5uM AlfB, or 5mM Mg/ATP (triangles) and 10uM AlfB (X's). To create a standardizing curve, buffer was added to the AlfA series instead of ATP (diamonds). After sedimentation of polymer at 80,000rpm for 20 minutes at 25 degrees C, supernatants were run on a Bis-Tris gradient acrylamide gel and the bands stained with SyproRed and visualized with a Typhoon scanner. The maximum concentration of AlfA remaining in the supernatant is equivalent to the critical concentration, which does not change dramatically after addition of AlfB, from 1.8uM in the absence of AlfB, to 2.2uM in the presence of 5uM AlfB, to 2.6uM in the presence of 10uM AlfB.

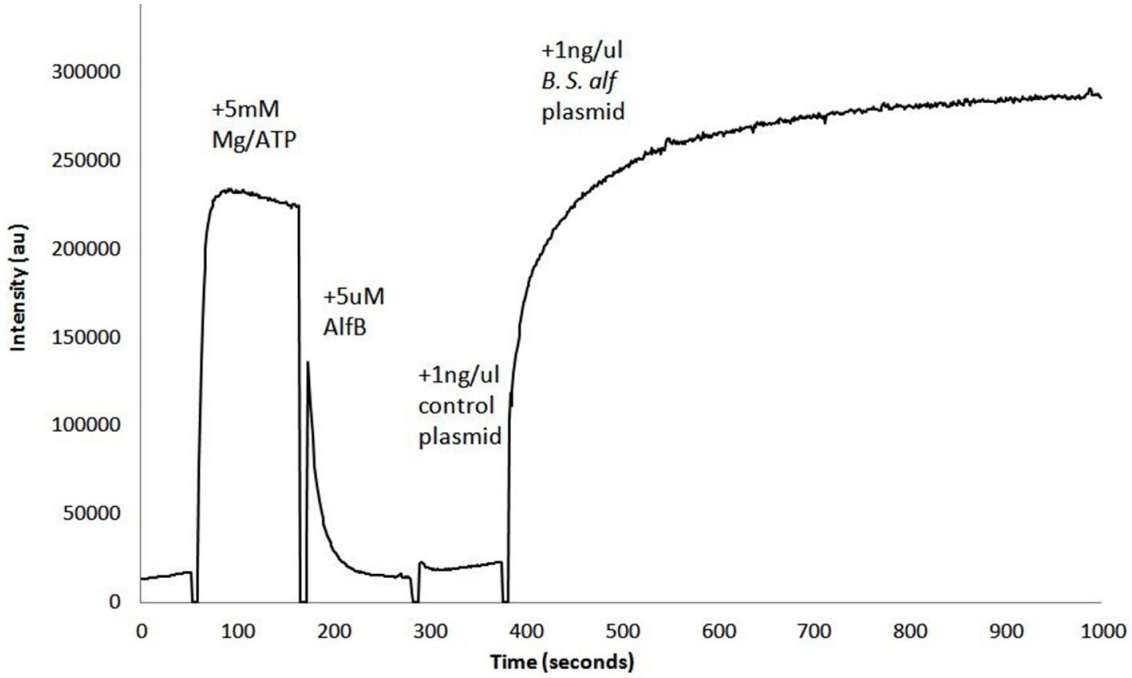

Figure 4. **Light scattering signal of AlfA is affected by addition of AlfB and ParN-containing DNA.** 3uM AlfA produces a right angle light scattering signal at 320 nm that dramatically increases upon addition of Mg/ATP due to polymerization of bundles. This signal drops dramatically after addition of an excess of AlfB (5uM), but can be recovered by addition of

plasmid DNA containing the *alf* operon at a concentration of 1ng/ul or approximately 20nm. A similar concentration of a cloning plasmid has no effect.

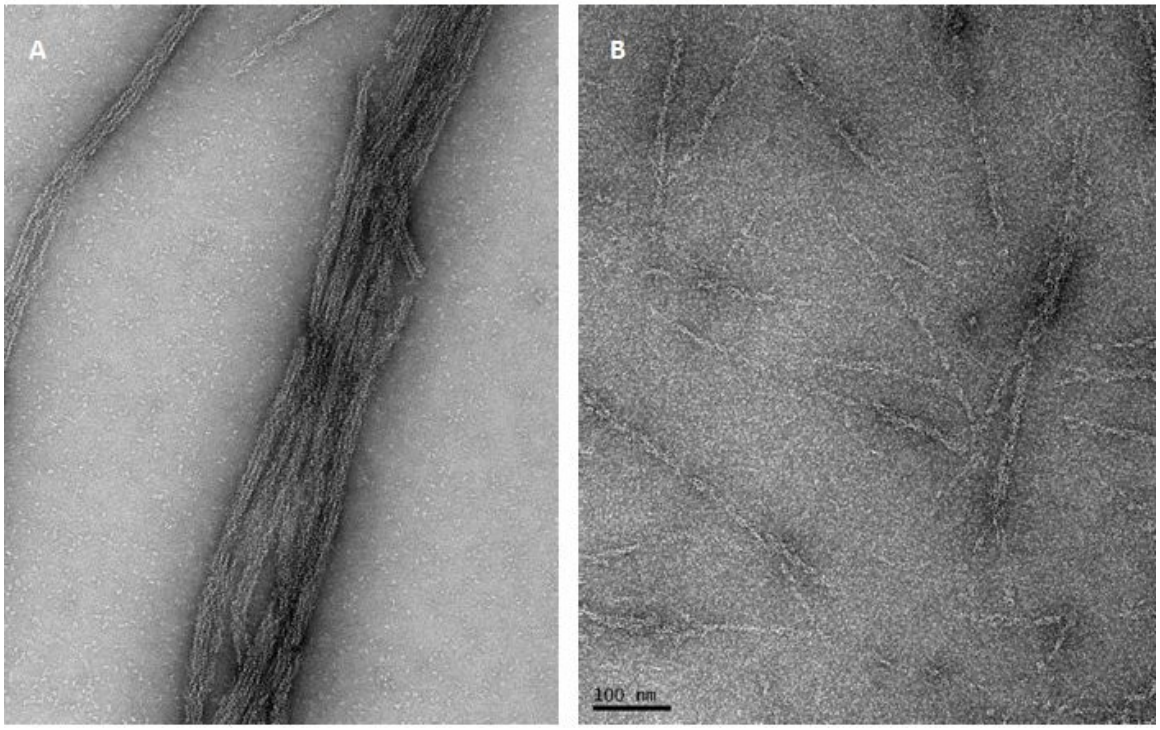

Figure 5. **The form of AlfA polymer changes in the presence of AlfB and DNA as visualized by EM.** 4.5uM AlfA was polymerized with 5mM Mg/ATP and, after incubation at room temperature for 10 minutes, stained with 0.75% uranyl formate for visualization by TEM. In the absence of AlfB (A) AlfA forms regular bundles, but these are disturbed by the addition of 5uM AlfB (B). Notably, this is the only condition other than >1.5M KCl that has been seen to cause the appearance of single filaments.

Spatial interaction of AlfA, AlfB, and ParN

While the light scattering and pelleting assays indicate that AlfB has an effect of AlfA that is modulated by the presence of specific DNA, it is difficult to make arguments about what

is happening to individual AlfA filament structures exposed to this complex. To address this question, we used negative stain EM and TIRF microscopy to observe individual bundles of AlfA. To visualize the DNA, we ordered a 5' primer with a Cy3 label, and a 3' primer with a biotin label. This DNA was coupled to streptavidin-coated magnetic beads which electron-dense (figure 6). In the presence of AlfA and AlfB, the majority of bundled filaments appeared to surround the beads, which were also connected to one another with bundles. In TIRF assays, however, these beads were mostly static, though they were frequently spaced apart from one another in a network (data not shown). DNA and streptavidin conjugates, however, were dynamic both along the filaments and tracking the growing ends of filaments (figure 7). The filaments also seemed to bundle with each other – two asters encountering one another on the glass (figure 8) annealed to one another much like individual bundles (chapter 2).

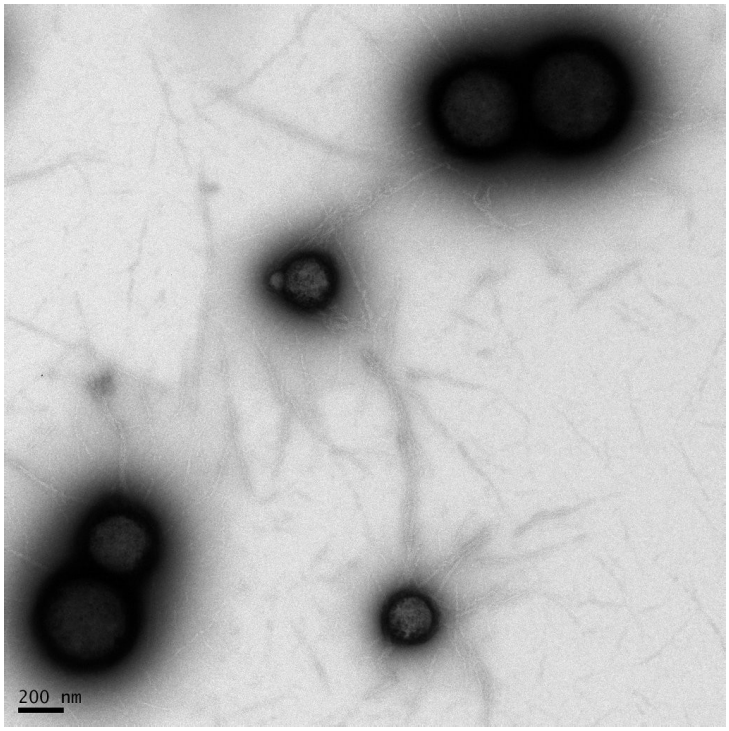

Figure 6. **AlfA polymer assembles on the surface of beads coated with ParN in the presence of AlfB.** 4.3uM AlfA was polymerized with 5mM Mg/ATP in the presence of 5uM AlfB and streptavidin-coated magnetic beads prebound with *parN*-biotin DNA. Negative stain EM

performed on a grid stained with 0.75% uranyl formate 30 seconds after polymerization shows that, while filaments do assemble in the background of this reaction, there is more polymer on the surface of the beads.

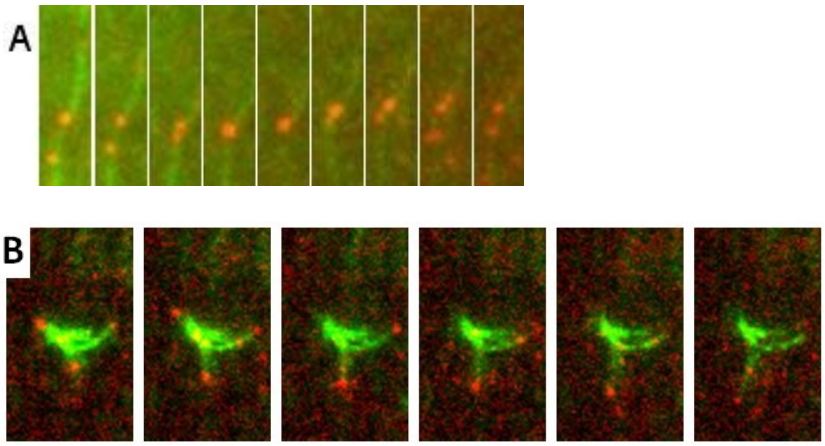

Figure 7. ***parN* DNA is moved by AlfA polymer in the presence of AlfB.** A bundle of AlfA filaments (green) binds to biotin- and Cy3-labeled *parN* DNA decorating streptavidin (red). These DNA particles move processively and bidirectionally along the AlfA structure (A), and also along the growing tips of AlfA filament ends (B), suggesting that insertional polymerization can drive this movement. Conditions: 3uM AlfA, 20% of which is labeled with Alexa488, in the presence of 5uM AlfB, 1% MC, and 15 mg/ml BSA. Time interval, 8 seconds (A), and 16 seconds (B).

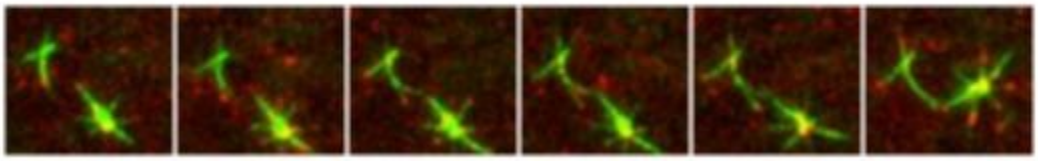

Figure 8. **DNA-coupled filaments can capture one another**. DNA-bound filament asters encounter one another in the 3rd frame. When the right aster becomes detached from the coverslip in the 6th frame, it remains attached to the left aster. This is likely the same type of lateral bundling capture interactions noted in TIRF experiments described in Chapter 2. Conditions are identical to those in figure 6. Time interval, 20 seconds.

Discussion

The preliminary characterization of AlfA posed many questions about the mechanism of segregation which were only partially answered by the *in vivo* experiments in chapter 3. From that work, we learned that AlfA plasmids can undergo bursts of directed motion (seen as short ballistic tracks and also an increase in α factor in MSD plots) that can correlated to filament polymerization (as seen as filament assembly behind a moving filament, or between separating filaments. These results suggested that AlfA filaments are pushed by filament polymerization, and that plasmids are non-randomly moved in the cell by their binding to a single structure that mechanically joins one plasmid to another that will move in the opposite direction. How this joining occurs, however, is still unclear. In the case of ParM, the dynamic instability and kinetic nonpolarity of individual filaments confers a necessity for *both* ends to be bound to plasmids in order to be stabilized. In this manner, the filament as a one dimensional, two-binding site structure specifies the geometry of segregation (Garner 2007).

In the case of AlfA filaments, which do not undergo dynamic instability, it is difficult to imagine how binding to a plasmid would confer additional stability that would cause preferential assembly over filaments in the background. Indeed, from the *in vivo* data, because of the small environment of the cell, it is essentially impossible to determine whether plasmids can simply bind to preexisting filaments, or if the filaments appear to be nucleated on plasmids. In this case, we also do not know how non-specific filament assembly would be discouraged. In either case, the mechanism of pairing one plasmid to another is also mysterious. Our preliminary TIRF data suggests that bundling may be a mechanism for this, but the lack of penetrance of our non-bundling mutant does not provide clarity.

We now have a partial answer to these questions from *in vitro* data. First, it appears that non-specific bundle assembly is discouraged by a relatively high molar ratio of AlfB to AlfA. Finally, the DNA-bound structures we have observed can anneal to one another by bundling and mechanically join two previously separate pieces of DNA together. This leads us to a model of DNA segregation detailed in figure 9 which relies on modulation of the formation of polymer bundles.

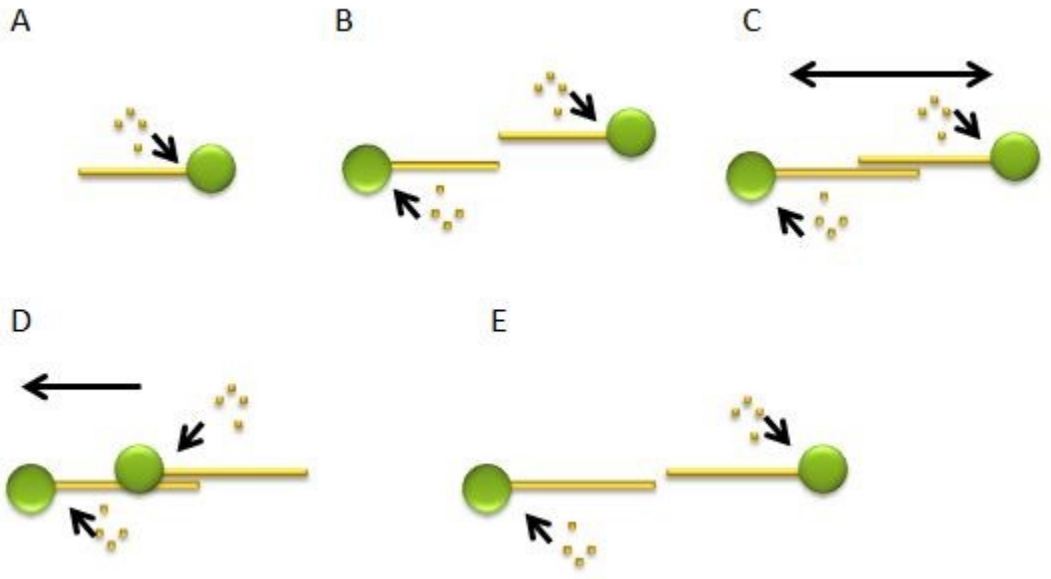

Figure 9. **Model for segregation**. Green circles represent plasmids, while yellow bar represents an AlfA filament that polymerizes from monomers (yellow squares). Plasmids are pushed via insertional polymerization of AlfA, as seen in TIRF experiments in figure 7 (A). When two filaments encounter each other, they can bundle together as in figure 8 (B). If this bundling occurs in an antiparallel fashion, insertional polymerization will drive the plasmids in opposite directions, increasing the space between them (C). If the bundling occurs in a parallel fashion, however, the space between the plasmids will be conserved instead of reduced, since the filaments will polymerize at the same speed (D). At some point, the bundles will fall apart due to turnover of individual filaments (E). Note that this model assumes that individual AlfA filaments

are polar: non-polar filaments would require a different mechanism of turnover (E) but would cause all bundling interactions to move plasmids in opposite directions. This model also assumes that interaction with the cell boundary does not stall filament polymerization (which would reduce the distance between plasmids attached to parallel bundles in D).

References

1. Garner, E. C., Campbell, C. S., Weibel, D. B. & Mullins, R. D. Reconstitution of DNA segregation driven by assembly of a prokaryotic actin homolog. *Science* **315**, 1270–1274 (2007).
2. Tanaka, T. Functional Analysis of the Stability Determinant AlfB of pBET131, a Miniplasmid Derivative of Bacillus subtilis (natto) Plasmid pLS32. *J. Bacteriol.* **192**, 1221–1230 (2010).

Chapter 5: Preliminary characterization of Alp7a

Introduction

Shortly after I began working on AlfA, Joe Pogliano's group published a phylogenetic analysis of dozens of newly-discovered actin-like proteins in bacteria, revealing that genes encoding homologues of this cytoskeletal protein exist not only on plasmids, but chromosomes and phage DNA as well (Derman, 2009). Since I had begun the project on AlfA with a desire to understand the scope of diversity in bacterial actin kinetics, structure, and mechanism, I was interested in having another data point to flesh out this parameter space. Working closely in collaboration with Alan Derman and enlisting the help of James Kraemer for crystallization studies, I initiated a project to purify and biochemically characterize Alp7a. The project is now in Natalie Petek's hands, but I have summarized my early findings below.

Purification of Alp7a

Alp7a can be purified almost identically to AlfA, as described above in chapter 2. However, the protein remains in the supernatant after a 50% ammonium sulfate cut. It can then be polymerized and pelleted directly from this supernatant. Care must be taken, however, due to the sensitivity of the polymer to ATP and magnesium (see below)

Structure of the polymer by negative stain EM

Alp7a forms regular polymers which assemble into what appear to be two dimensional sheets (see figure 1). The sheets become larger and more regular with time, reaching an apparent maximum width of approximately 80nm after 1 hour polymerization. At early time

points (30 seconds after polymerization) the sheets are more narrow and less regular, but I never observed single filaments.

The sheets were very regular, and reference free averages (using EMAN as described above for AlfA) reflect this (figure 2). The references show discrete strands of Alp7a with structural features resembling lobes. These lobes can be open or closed, but in each class, all lobes appear to be rotated comparably. This confers a polarity to these filaments, and strikingly, the filaments in each class appear to be running antiparallel to their neighbors (most obvious in classes 0, 1, 5, and 7), suggesting that the Alp7a sheets are comprised of filaments of alternating polarity.

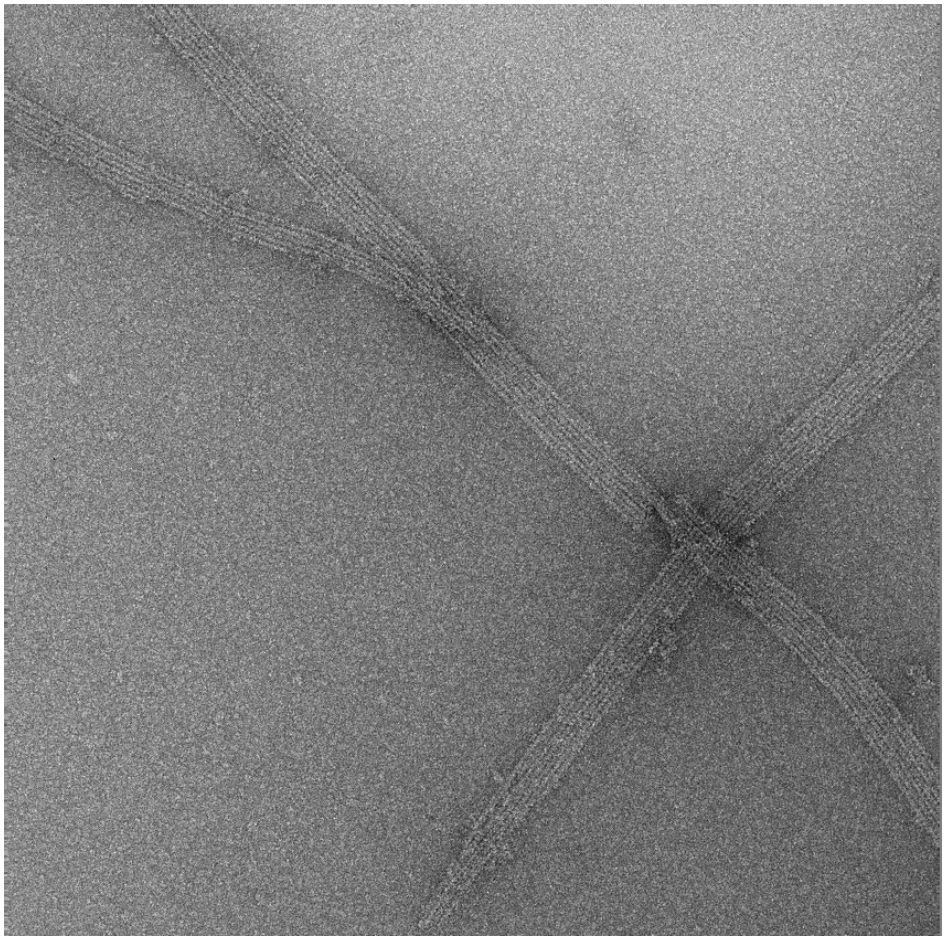

Figure 1**. Negative stain of Alp7a.** 25uM Alp7a polymer approximately 20 minutes after assembly was stained with 0.75% Uranyl formate. The sheets in this image are approximately 50nm wide.

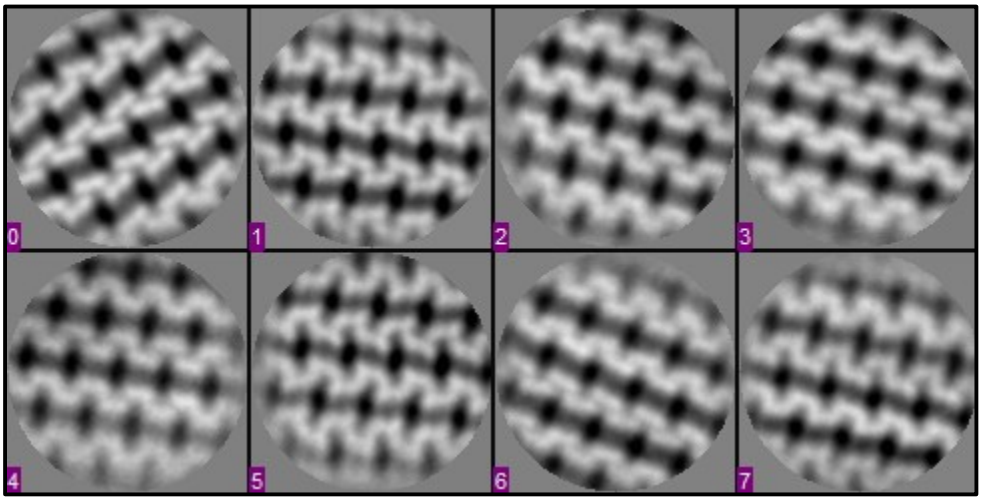

Figure 2. **Reference free averages of Alp7a sheets from negatively stained EM**. Each class represents approximately 200 images.

Recalcitrant assembly: high critical concentration and sensitivity to ATP and Magnesium

Alp7a assembly kinetics are markedly different from that of ParM or AlfA. For example, I measured the critical concentration of Alp7a to be 13.6uM, far higher than the 2.3-2.4uM for AlfA or ParM. I also found that Alp7a was very sensitive to the concentration of magnesium in solution. While AlfA or ParM will polymerize with less magnesium in solution than ATP, Alp7a requires magnesium to be in excess of ATP (suggesting perhaps that the affinity of Alp7a for magnesium is lower than the affinity of ATP for magnesium). Polymerization was optimal with 2mM excess of magnesium.

In addition, Alp7a also requires a higher concentration of ATP for assembly (figure 3), suggesting that its affinity for nucleotide is also modest. This feature may contribute to its

amenability to crystallization (figure 4), since crystallization of many cytoskeletal polymers is stymied by polymerization (Justin Kollman, personal communication).

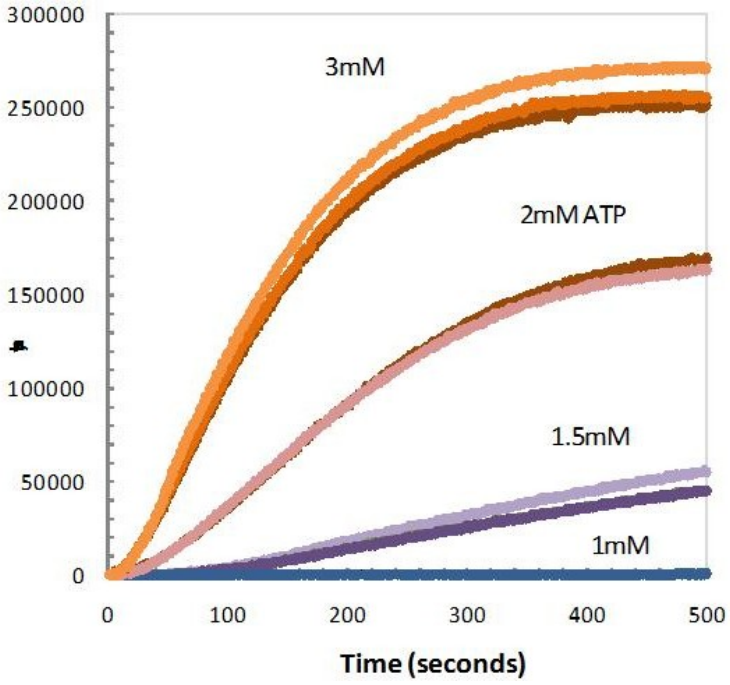

Figure 3. **Sensitivity of Alp7a to ATP concentration.** 16.3uM Alp7a was polymerized in the presence of 5mM MgCl2 and varying concentrations of ATP (text on graph). Light scattering intensity is represented in arbitrary units on the vertical axis.

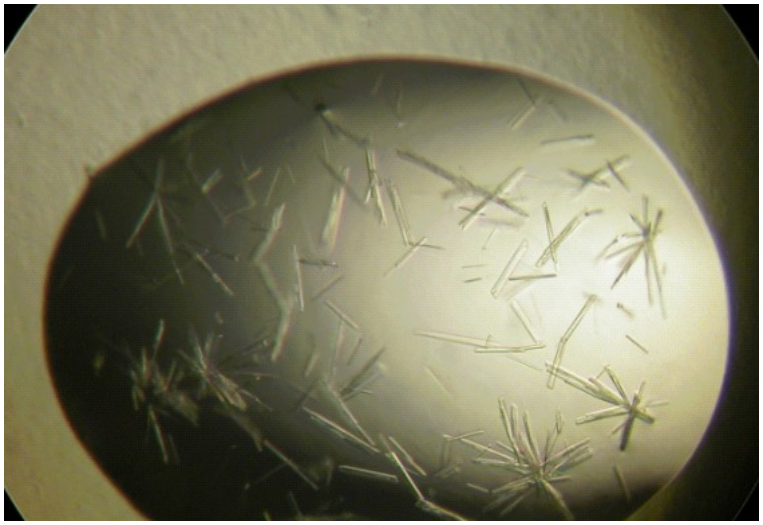

Figure 4. **Initial crystallization hits of Alp7a.** Approximately 10% of 800 conditions initially tested with a mosquito screen performed by James Kraemer resulted in small crystals with needle- or aster-like morphology.

Discussion

The assembly features of Alp7a polymer in isolation, especially the high critical concentration, recall observations made *in vivo* (Derman, 2009). Specifically, the authors expressed Alp7a from an inducible promoter, allowing them to titrate levels of the protein in *Bacillus subtilis*. They found that in the absence of other components of the Alp7 operon (Alp7r, a downstream DNA-binding protein, and the DNA-binding region) a markedly higher concentration of inducer needed to be used to see polymer formation. This suggests that the Alp7a critical concentration is depressed by other factors, which makes sense in the light of the very high critical concentration observed *in vitro*. Interestingly, the polymer that did form in the absence of other factors appeared thicker and were static – perhaps being composed of bundle or sheet. In the presence of the full operon, Alp7a polymers appear thinner and can be seen to undergo various dynamics, including treadmilling. Given that treadmilling requires different on and off rates at both ends of the structure, this is a behavior that would be difficult to explain from a bundle of antiparallel filaments. Together, these findings suggest that studying the polymer in isolation will not explain the mechanisms seen *in vivo*. It suggests that the addition of other regulators, namely Alp7r and perhaps the DNA sequence to which it binds, will dramatically alter the assembly of this polymer.

References

1. Derman, A. I. *et al.* Alp7R Regulates Expression of the Actin-Like Protein Alp7A in Bacillus subtilis. *J. Bacteriol.* **194**, 2715–2724 (2012).

2. Derman, A. I. *et al.* Phylogenetic analysis identifies many uncharacterized actin-like proteins (Alps) in bacteria: regulated polymerization, dynamic instability and treadmilling in Alp7A. *Molecular Microbiology* **73**, 534–552 (2009).

Appendix: Permissions

LAST UPDATED: November 5, 2009

ASM Journals Statement of Authors' Rights

Authors may post their articles to their institutional repositories

ASM grants authors the right to post their accepted manuscripts in publicly accessible electronic repositories maintained by funding agencies, as well as appropriate institutional or subject-based open repositories established by a government or non-commercial entity. Since ASM makes the final, typeset articles from its primary-research journals available free of charge on the ASM Journals and PMC websites 6 months after final publication, ASM recommends that when submitting the accepted manuscript to PMC or institutional repositories, the author specify that the posting release date for the manuscript be no earlier than 6 months after the final publication of the typeset article by ASM.

Authors may post their articles in full on personal or employer websites

ASM grants the author the right to post his/her article (after publication by ASM) on the author's personal or university-hosted website, but not on any corporate, government, or similar website, without ASM's prior permission, provided that proper credit is given to the original ASM publication.

Authors may make copies of their articles in full

Corresponding authors are entitled to 10 free downloads of their papers. Additionally, all authors may make up to 99 copies of his/her own work for personal or professional use (including teaching packs that are distributed free of charge within your own institution). For

orders of 100 or more copies, you should seek ASM's permission or purchase access through Highwire's Pay-Per-View option, available on the ASM online journal sites.

Authors may republish/adapt portions of their articles

ASM also grants the authors the right to republish discrete portions of his/her article in any other publication (including print, CD-ROM, and other electronic formats) of which he or she is author or editor, provided that proper credit is given to the original ASM publication. "Proper credit" means either the copyright lines shown on the top of the first page of the PDF version, or "Copyright © American Society for Microbiology, [insert journal name, volume number, year, page numbers and DOI]" of the HTML version. You may obtain permission from Rightslink. For technical questions about using Rightslink, please contact Customer Support via phone at (877) 622-5543 (toll free) or (978) 777-9929, or e-mail Rightslink customer care at **customercare@copyright.com.**

Please note that the ASM is in full **compliance with NIH Policy.**

Publishing Agreement

It is the policy of the University to encourage the distribution of all theses, dissertations, and manuscripts. Copies of all UCSF theses, dissertations, and manuscripts will be routed to the library via the Graduate Division. The library will make all theses, dissertations, and manuscripts accessible to the public and will preserve these to the best of their abilities, in perpetuity.

I hereby grant permission to the Graduate Division of the University of California, San Francisco to release copies of my thesis, dissertation, or manuscript to the Campus Library to provide access and preservation, in whole or in part, in perpetuity.

August 1, 2012

Author signature *Date*